

To appear in ApJ, NN.

## IR Surface Brightness Fluctuations of Magellanic Star Clusters<sup>1</sup>

Rosa A. González<sup>2</sup>

*Centro de Radioastronomía y Astrofísica, UNAM, Campus Morelia, Michoacán, México, C.P.  
58190*

Michael C. Liu<sup>3</sup>

*Institute for Astronomy, University of Hawaii, 2680 Woodlawn Drive, Honolulu, HI 96822*

and

Gustavo Bruzual A.<sup>4</sup>

*Centro de Investigaciones de Astronomía, Apartado Postal 264, Mérida 5101-A, Venezuela*

### ABSTRACT

We present surface brightness fluctuations (SBFs) in the near-IR for 191 Magellanic star clusters available in the Second Incremental and All Sky Data releases of the Two Micron All Sky Survey (2MASS), and compare them with SBFs of Fornax Cluster galaxies and with predictions from stellar population models as well. We also construct color-magnitude diagrams (CMDs) for these clusters using the 2MASS Point Source Catalog (PSC). Our goals are twofold. First, to provide an empirical calibration of near-IR SBFs, given that existing stellar population synthesis models are particularly discrepant in the near-IR. Second, whereas most previous SBF studies have focused on old, metal rich populations, this is the first application to a system with such a wide range of ages ( $\sim 10^6$  to more than  $10^{10}$  yr, i.e., 4 orders of magnitude), at the same time that the clusters have a very narrow range of metallicities ( $Z \sim 0.0006 - 0.01$ , ie., 1 order of magnitude only). Since stellar population synthesis models predict a more complex sensitivity of SBFs to metallicity and age in the near-IR than in the optical, this analysis offers a unique way of disentangling the effects of age and metallicity.

---

<sup>1</sup>This research has made use of the NASA/ IPAC Infrared Science Archive, which is operated by the Jet Propulsion Laboratory, California Institute of Technology, under contract with the National Aeronautics and Space Administration.

<sup>2</sup>E-mail address: `r.gonzalez@astrosmo.unam.mx`

<sup>3</sup>E-mail address: `mliu@ifa.hawaii.edu`

<sup>4</sup>E-mail address: `bruzual@cida.ve`

We find a satisfactory agreement between models and data. We also confirm that near-IR fluctuations and fluctuation colors are mostly driven by age in the Magellanic cluster populations, and that in this respect they constitute a sequence in which the Fornax Cluster galaxies fit adequately. Fluctuations are powered by red supergiants with high-mass precursors in young populations, and by intermediate-mass stars populating the asymptotic giant branch in intermediate-age populations. For old populations, the trend with age of both fluctuation magnitudes and colors can be explained straightforwardly by evolution in the structure and morphology of the red giant branch. Moreover, fluctuation colors display a tendency to redden with age that can be fit by a straight line. For the star clusters only,  $(\bar{H} - \bar{K}_s) = (0.21 \pm 0.03)\text{Log}(\text{age}/\text{yr}) - (1.29 \pm 0.21)$ ; once galaxies are included,  $(\bar{H} - \bar{K}_s) = (0.20 \pm 0.02)\text{Log}(\text{age}/\text{yr}) - (1.25 \pm 0.16)$ . Finally, we use for the first time a Poissonian approach to establish the error bars of fluctuation measurements, instead of the customary Monte Carlo simulations.

*Subject headings:* astronomical data bases: miscellaneous — galaxies: distances and redshifts — galaxies: star clusters — Magellanic Clouds — stars: AGB and post-AGB

## 1. Introduction

While the mean surface brightness of a galaxy is independent of distance, the variance about the mean decreases with distance — i.e., given the same angular resolution, more distant galaxies appear smoother. This is the principle behind surface brightness fluctuation measurements (SBFs; Tonry & Schneider 1988; Blakeslee, Vazdekis, & Ajhar 2001), one of the most powerful methods to determine cosmological distances (e.g., Tonry et al. 1997; Liu & Graham 2001; Jensen et al. 2003). SBFs arise from Poisson fluctuations in the number of stars within a resolution element, and they are measured through the observed ratio of the variance to the mean surface brightness of a galaxy; that is, the ratio (denoted  $\bar{L}$ ) of the second to the first moment of the stellar luminosity function, scaled by the inverse of  $4\pi d^2$ , where  $d$  is the distance. SBF measurements are expressed in  $\bar{m}$  and  $\bar{M}$ , which are, respectively, the apparent and absolute magnitudes of  $\bar{L}$ .

SBF magnitudes, however, depend not only on galaxy distances, but also on the age and metallicity of stars. Therefore, SBFs also offer a unique possibility to investigate unresolved stellar populations. For example, as a luminosity-weighted mean,  $\bar{M}$  is much more sensitive to giant stars than integrated colors (Worley 1993a; Ajhar & Tonry 1994). For the same reason,  $\bar{M}$  is relatively insensitive to differences in the IMF for intermediate-age and old systems.

We engaged in this work with the aim of providing an empirical calibration of near-IR SBFs, specifically for the study of unresolved stellar populations. The near-IR is very favorable for SBF measurements, from the point of view of improved signal (the light of intermediate and old populations is dominated by the asymptotic giant branch, AGB, and the red giant branch, RGB), reduced dust extinction and, last but not least, the model prediction that near-IR SBFs might help break the

age–metallicity degeneracy (Worley 1993b). However, there is the very important disadvantage that existing stellar population synthesis models are particularly discrepant in the near–IR spectral region (Charlot, Worley, & Bressan 1996; Liu, Charlot, & Graham 2000; Blakeslee, Vazdekis, & Ajhar 2001). The disagreement is as high as  $\sim 0.2$  mag in  $(V - K)$ , compared to  $\sim 0.05$  mag in  $(B - V)$ . The ill–determined contribution of asymptotic giant branch (AGB) stars to the integrated light may be the most important source of this problem (Ferraro et al. 1995). Such an uncertainty is bound to compromise the calibration of  $\bar{M}$ . *An empirical calibration of near–IR SBFs is therefore essential.*

## 2. Our strategy

In theory, a good starting point to assess the impact of stellar population variations on SBFs, and to empirically calibrate  $\bar{M}$  would be to derive fluctuations for a number of simple stellar populations with known distances. This is not a new idea. Ajhar & Tonry (1994) attempted to calibrate the SBFs zero–point with  $V$  and  $I$  photometry of Galactic globular clusters. Their derived  $\bar{M}_I$ , however, does not constrain  $\bar{M}_I$  for galaxies, since the range of ages of Galactic globular clusters is small, and in general their metallicities do not overlap with those of spiral bulges and early–type galaxies. About five (Harris 1996) of the inner–disk subgroup of the Galactic globular clusters have metallicities in the right range; aside from the fact that ages and distances of those clusters are generally not very well determined yet, their number is so small that their analysis will be dominated by stochastic effects (see §4). Finally, Ajhar & Tonry (1994) found that optical data alone are inadequate to decouple the effects of age and metallicity reliably.

A study of the Magellanic Clouds (MC) clusters would seem to constitute a better course of action from the point of view of their relevance to early–type galaxies, for two reasons: the clusters have very well known distances, and they span a much wider range of ages ( $\sim 10^6$  to  $\sim 10^{10}$  yr) than the Galactic globular clusters (all with  $\sim 10^{10}$  yr). The oldest MC clusters are as old or older than elliptical galaxies and spiral bulges. On the other hand, it is true that their metallicity is low ( $Z \sim 0.0006 - 0.01$ ), but their slow chemical enrichment history means that clusters with ages between a few Myr and 3 Gyr have all basically  $Z \sim 0.01$  (Cohen 1982). Since stellar population synthesis models predict a more complex sensitivity to metallicity and age in the near–IR than in the optical SBFs (Worley 1993a; Liu, Charlot, & Graham 2000), a near–IR study of the MC star clusters, with their wide range of ages (4 orders of magnitude) and narrow range of metallicities (1 order of magnitude only), could offer a unique way of disentangling the effects of age and metallicity.

In reality, for this approach to work, the sample should include as many clusters as possible, because it is in star clusters where the AGB problem manifests itself most dramatically. In each individual cluster, the stars populating the AGB and the upper red giant branch (RGB) are so few that they do not properly represent the distribution of the brightest AGB/RGB stars on the isochrone. Often, the integrated near–IR light and, even worse, the SBFs will be dominated by a single luminous, cool star. The way around this problem is an appropriate treatment of a

sufficiently rich database. Fortunately,  $J$ ,  $H$ , and  $K_s$  data of all MC clusters are now available in the Two Micron All Sky Survey (2MASS; Skrutskie et al. 1997). Rather than analyzing each cluster separately, in order to reduce stochastic effects we have built “superclusters,” by coadding clusters in the Elson & Fall (1985, 1988) sample that have the same SWB class (Searle, Wilkinson, & Bagnuolo 1980). The SWB classification is based on two reddening-free parameters, derived from integrated  $ugvr$  photometry of 61 rich star clusters in the Magellanic Clouds; it constitutes a smooth, one-dimensional sequence of increasing age and decreasing metallicity. Elson & Fall (1985) assigned SWB classes to 147 more clusters using  $UBV$  photometry, assuming a low and uniform reddening ( $E_{B-V} \approx 0.1 \pm 0.1$ ) towards and in the clouds, which is valid in general for clusters older than a few times  $10^7$  years (Charlot & Fall 2000). The Elson & Fall (1985) classification is parameterized by  $s$ , where  $s = (5.75 \pm 0.26)$  SWB class +  $(9.54 \pm 1.45)$ . We have grouped the clusters in superclusters according to their  $s$ -parameter, rather than their SWB class, as shown in Table 1. Nevertheless, we have assigned ages and metallicities to the superclusters from Cohen (1982), by virtue of their SWB types.<sup>5</sup>

In order to compare the results obtained for star clusters with those for galaxies, we use  $\bar{M}_{K_s}$  and  $\bar{M}_{F160W}$  derived for a sample of Fornax Cluster galaxies by, respectively, Liu, Graham, & Charlot (2002) and Jensen et al. (2003). Likewise, we have taken the  $J$ ,  $H$ , and  $K_s$  integrated fluxes and colors of the Fornax galaxies directly from the 2MASS Second Incremental Release Extended Source Catalog (XSC), via the GATOR catalog web query page. Finally, ages and abundances have been adopted from Kuntschner (1998). Parameter values for the Fornax Cluster galaxies are all presented in Table 2.

We had to convert  $\bar{M}_{F160W}$  of the galaxies to  $\bar{M}_H$ . From the photometric transformations between the *HST* NICMOS Camera 2 filters and the CIT/CTIO system, published by Stephens et al. (2000) for cool giants of near-solar metallicity, we get:

$$m_H = m_{F160W} + (0.080 \pm 0.069) - (0.243 \pm 0.046)(m_J - m_K). \quad (1)$$

However, the transformation coefficients for fluctuation magnitudes may be different from these, since the spectrum of the fluctuations is not the same as the spectra of the stars used to derive the transformation. Buzzoni (1993) –for transformations of SBF magnitudes between Johnson  $R$ ,  $I$ , and Cousins  $R$ ,  $I$ – and Blakeslee, Vazdekis, & Ajhar (2001) –for transformations between  $V_{F555W}$ ,  $I_{F814W}$ , and Johnson  $V$ , Cousins  $I$ – maintain that transformation equations obtained from stellar observations can be used for fluctuation magnitudes of galaxies if fluctuation colors are substituted for integrated ones. On the other hand, Tonry et al. (1997) state that, instead, the mean ( $V - I$ ) color of the fluctuations –which these authors use to correct their SBF magnitudes– is the mean of the integrated color and the fluctuation color ( $\bar{V} - \bar{I}$ ). In view of these conflicting statements, we

---

<sup>5</sup>The exception is the Pre-SWB supercluster, for which we have assumed the age of a cluster with  $s=7$ , or the “central”  $s$ -type of its constituents.

have used models (see §4) to decide which color is most appropriate to use in the above equation to transform  $\overline{F160W}$  to  $\bar{H}$ . For model populations with solar metallicity and  $Z = 0.05$  —the most relevant metallicities for the galaxies—, we have plotted in Figure 1 ( $\bar{H} - \overline{F160W}$ ) vs  $(J - K)$ ,  $(\bar{J} - \bar{K})$ , and integrated  $(J - K)_{bright}$  of stars brighter than  $M_K \leq -4.5$  (which are the ones we can detect as resolved sources at the distance of the LMC and which mostly determine the fluctuation values, see §3). Model transformations are closest to equation 1 when using the color of the brightest stars, which also turns out to be approximately the mean of the integrated  $(J - K)$  and  $(\bar{J} - \bar{K})$ , as described by Tonry et al. (1997). Since we do not have  $K$  for the galaxies, but  $K_s$ , we have also used the models to check that the uncertainty introduced by using  $K_s$  is smaller than the systematic error made when applying the stellar transformation to the  $\overline{F160W}$  measurements. Of course, we cannot measure  $(J - K_s)_{bright}$  directly but, from the models, it is approximately 0.48 mag redder than the integrated  $(J - K_s)$  for the color range of the galaxies (0.85 – 0.95). (Unfortunately, we do not have  $(\bar{J} - \bar{K}_s)$  for the galaxy data, so we cannot derive empirically the mean  $(J - K_s)$  color of the fluctuations, either.) Summarizing, we use the following transformation equation:

$$\bar{M}_H = \bar{M}_{F160W} + (0.08 \pm 0.07) - (0.24 \pm 0.05)(J - K_s + 0.48). \quad (2)$$

### 3. Treatment of the data

As stated above,  $\bar{L}$  is the ratio of the second moment of the luminosity function to its first moment, the integrated luminosity. This can be expressed with the following equation:

$$\bar{L} \equiv \frac{\sum n_i L_i^2}{\sum n_i L_i}, \quad (3)$$

where  $n_i$  is the number of stars of type  $i$  and luminosity  $L_i$ . Bright stars are the main contributors to the numerator, while faint stars contribute significantly to the denominator. In contrast to the measurements performed in distant galaxies, where pixel-to-pixel SBFs probe unresolved stellar populations, in star clusters the second moment of the stellar luminosity function, or the numerator, is derived from measurements of resolved, bright stars (Ajhar & Tonry 1994). The integrated luminosity or the denominator, on the other hand, is equal to the total light detected in the image, after removal of any sky background emission. The depth of the 2MASS survey is more than adequate for our purposes. In the optical and at least for Galactic halo globulars, the second moment of the luminosity converges quickly, with 99% of the sum being obtained with the three brightest magnitudes of cluster stars (Ajhar & Tonry 1994). The southern 2MASS survey was carried out with a 1.3-m telescope at the Cerro Tololo Inter-American Observatory (CTIO); the  $J$ ,  $H$ , and  $K_s$  data were secured simultaneously with a 3-channel camera, equipped with three  $256 \times 256$  NICMOS3 arrays. The seeing throughout the 2MASS observations ranged —respectively for  $J$ ,  $H$ , and  $K_s$ — from  $2''.4$  to  $5''.4$ ,  $2''.5$  to  $5''.0$ , and  $2''.5$  to  $4''.6$ ; the average seeing was  $2''.8$  for

$J$  and  $K_s$ , and  $2''.7$  for  $H$ .<sup>6</sup> The raw camera pixel size of the survey was  $2''$ , but the sampling was improved by dithering. The released data have  $1''$  pixels, and we have measured an average FWHM of  $3''$ , in all three bands. Nominally, the 2MASS PSC is 100% complete for  $K_s < 15$  mag at the general position of the Magellanic Clouds.<sup>7</sup> To err on the conservative side, though, we have inspected the luminosity functions of the clusters within  $1'$  of their centers. Eighty seven per cent of them seem complete for  $K_s < 14$  mag; this means that the four brightest magnitudes of stars at the distance of the Large Magellanic Cloud (LMC) have been detected (see Fig. 3). In §4 below, we demonstrate that these should suffice for the calculation of fluctuation magnitudes and colors in the near-IR.

We retrieved from the 2MASS archive  $J$ ,  $H$ , and  $K_s$  data for 156 MC clusters with an  $s$ -parameter (Elson & Fall 1985, 1988), and that were available in the Second Incremental Release of the 2MASS database as Atlas (i.e., uncompressed) images. Later, we obtained images restored from lossy-compressed files for another 35 clusters from the All Sky release. The data were then used to build eight “superclusters,” one for each of the seven different SWB classes (Searle, Wilkinson, & Bagnuolo 1980), plus one “Pre-SWB-class” supercluster. Besides the images, photometry for the point sources was obtained from the 2MASS Second Incremental Release and All-Sky PSCs; the coordinates used to retrieve the source lists were mostly those provided by SIMBAD, although for many of the Small Magellanic Cloud (SMC) objects we used the coordinates in Welch (1991) and, occasionally, positions determined from the  $J$  images by eye. At this stage, the  $J$  photometry was used to find a center of light for all the images.

Once centered, we proceeded to assemble the supercluster mosaics by coadding the individual clusters of each SWB class, after subtracting the sky value registered in the image header,<sup>8</sup> multiplicatively scaling each one to a common photometric zero-point, dereddening (even though reddening is not very important at these wavelengths), and geometrically magnifying SMC clusters to place all of them at the same distance modulus of the LMC. We take  $(m - M)_o = 18.50 \pm 0.13$  for the LMC, and  $(m - M)_o = 18.99 \pm 0.05$  for the SMC,<sup>9</sup> after the Cepheid distances in Ferrarese et al. (2000). We also masked out bad columns. An important final step was to correct for any residual over or undersubtraction of the sky emission, by measuring the background of each supercluster mosaic in an annulus between  $2'.0$  and  $2'.5$  from the center. The mosaics were used mainly

---

<sup>6</sup><http://spider.ipac.caltech.edu/staff/roc/2mass/seeing/seesum.html>

<sup>7</sup>[http://www.ipac.caltech.edu/2mass/releases/allsky/doc/sec2\\_2.html](http://www.ipac.caltech.edu/2mass/releases/allsky/doc/sec2_2.html)

<sup>8</sup>For several of the clusters, we confirmed the accuracy of this value by eye, by looking at the mode in an annulus between  $2'.0$  and  $2'.5$  from the cluster center, and with DAOPHOT (Stetson 1987).

<sup>9</sup>The errors listed in Tables 3 and 4 for the derived absolute integrated and fluctuation magnitudes of the MC superclusters do not include the quoted errors in the clouds’ distance moduli, nor dispersions due to their depths along the line of sight. Neither should affect the conclusions of this study. The *systematic* error in the *HST* Cepheid distance to the LMC, estimated to be about  $\pm 0.16$  mag (Mould et al. 2000), is also not taken into account; future adjustments to the LMC distance modulus would result in a constant offset applied to the SBF absolute magnitudes of the Fornax galaxies we have taken from the literature and of the MC superclusters that we derive here.

to measure the integrated light of the superclusters, a quantity that goes into the denominator of the expression for  $\bar{L}$ . With the aid of a few star clusters for which both uncompressed and compressed images were available, we checked that the compressed ones were adequate to perform these measurements, for the few cases where only the latter were released. We also inspected the radial profiles of the mosaics in order to look for anomalies (e.g. extremely bright, probably foreground, stars) and to assess the contribution to the integrated light from different radii.

Next, we went back to the PSC in order to assemble star lists for each supercluster.<sup>10</sup> This time, the star lists for the individual clusters were retrieved with VizieR (Ochsenbein, Bauer, & Marcout 2000) using the centers determined from the  $J$  light centroids. Afterwards, the distance of each star from the center of the supercluster was adjusted to account for the differences in distance among the clouds, again to place all the stars at a distance modulus of  $(m - M)_o = 18.50$ ; the photometry, too, was corrected for the differences in distance, as well as for reddening. Finally, sources with dubious photometry were eliminated, as were outliers. To evaluate the quality of the photometry, we used the flags from the PSC itself. We kept only sources within  $1'$  from the centers of the superclusters; that had been detected and had no artifacts in all three bands; that had read-out-2 – read-out-1 profile-fit photometry,<sup>11</sup> also at  $J$ ,  $H$ , and  $K_s$ ; and that were not associated with either an extended source, a minor planet, or a comet. In order to minimize field contamination, we followed the criterion of Ferraro et al. (1995), that is, we excluded from the analysis stars in the range  $12.3 < (K_s)_o < 14.3$  with colors  $(J - K_s)_o > 1.2$  or  $(J - K_s)_o < 0.4$ . Given that the radius of 1 arcmin encompasses only the centers of the star clusters, no further field decontamination scheme was applied.

Out of these starlists, three CMDs were produced for each supercluster, one for stars with  $r < 0\rlap{.}^{\prime}34$ , a second one for stars with  $0\rlap{.}^{\prime}34 \leq r < 0\rlap{.}^{\prime}66$  and, finally, another one for stars with  $0\rlap{.}^{\prime}67 \leq r \leq 1\rlap{.}^{\prime}0$ . The comparison between the 3 diagrams of each supercluster reassured us that field contamination was not a problem. We got rid of probable foreground stars: one extremely bright star in NGC 1754 (SWB VI), another in NGC 1786 (SWB VII), and a couple of bright, blue, stars in NGC 1777 (SWB V).

---

<sup>10</sup>For several of the individual star clusters, we verified the accuracy of the published photometry with DAOPHOT. As an external check, the near-IR photometry obtained by Ferraro et al. (1995) for 12 globular clusters in the Magellanic Clouds is virtually identical to their PSC raw (i.e., dismissing quality flags) photometry; when using the flags to eliminate sources, the CMDs produced with the PSC values are tighter than those published by Ferraro and collaborators. These authors obtained their data with the 1.5-m telescope at CTIO and an InSb array,  $58 \times 62$  pixel, with a pixel size of  $0\rlap{.}^{\prime}92$ . It is perhaps worth mentioning that the similarity between the PSC and the Ferraro et al. (1995) results is what convinced us in the first place that this project could be done with the 2MASS data.

<sup>11</sup>The integration time for each frame in the 2MASS survey included: two 51 ms resets, one 51 ms “Read\_1” (R1) integration, and one 1.3 s “Read\_2” (R2) integration. An additional delay of 5 ms was added to allow for overhead and settling. 2MASS Atlas images were produced by the coaddition of six overlapping R1 – R2 frames, each with 1.3 s integration, for a total integration time of 7.8 s. Point sources were detected from the Atlas images, but the position and photometry of faint sources (most sources in the catalog) were estimated through profile-fitting in each of the six stacked R1 – R2 frames (Cutri et al. 2003).

Lastly, integrated fluxes, integrated colors, absolute fluctuation magnitudes, and fluctuation colors were obtained for each supercluster. The integrated fluxes, which are also needed for the denominator of eq. 3, were acquired simply by summing up the flux in all the pixels within  $1'$  of the center of each supercluster, and subtracting the flux from foreground stars and from bright stars (i.e., sources in the PSC catalog with  $K_s \leq 14$  at the distance of the LMC) that had dubious photometry, as judged from the PSC flags; this is mathematically analogous, but procedurally much easier, than measuring each separate cluster image and then adding. The numerator of eq. 3, on the other hand, was calculated by performing sums over the individual stars with good photometry in the same region.

We present in Figure 2 images of all eight superclusters. These are greyscale versions of  $J$ ,  $H$ , and  $K_s$  color mosaics. Figure 3 displays, again for all superclusters, the CMDs of the stars within  $1'$  of their centers. The average photometric errors are 0.04 mag in brightness and 0.02 mag in color for sources with  $K_s \leq 13$ ; respectively, 0.06 and 0.03 mag for stars with  $13 < K_s \leq 14$ ; and 0.13 and 0.07 mag (about the size of the dots) for sources with  $14 < K_s \leq 15$ . The width of several of the diagrams (conspicuously, II and III) results from the fact that our artificial clusters are not fully homogeneous populations; unfortunately, binning the data in superclusters is the compromise we have found most convenient to adopt in order to try to circumvent the problem of small number statistics posed by individual star clusters (c.f. §2 and §4). As we will see below (§5), this approach lets the general tendencies of the data show through, while hopefully eliminating possible biases and reducing random errors.

Table 1 lists assumed age and metallicity of the superclusters; limiting radii of analyzed regions (in arcseconds *at the distance of the LMC*); star clusters that went into building each supercluster; number of stars of each individual cluster that contributed to the calculation of the supercluster SBFs;  $s$ -parameter from Elson & Fall (1985) or Elson & Fall (1988); whether the star clusters belong to the LMC or the SMC;  $E(B - V)$  from Persson et al. (1983); and SWB-class from Searle, Wilkinson, & Bagnuolo (1980). When clusters do not have individually measured reddening, we have assumed  $E(B - V) = 0.075$  for the LMC and  $E(B - V) = 0.037$  for the SMC (Schlegel et al. 1998); also from Schlegel et al. (1998), we have taken  $A_J = 0.902E(B - V)$ ,  $A_H = 0.576E(B - V)$ , and  $A_K = 0.367E(B - V)$ .

#### 4. Models and errors

We use the most recent Bruzual & Charlot (2003) evolutionary stellar population synthesis models. Here, we utilize what these authors call the “standard” reference models for different metallicities, built using the Padova 1994 stellar evolution isochrones (Alongi et al. 1993; Bressan et al. 1993; Fagotto et al. 1994a,b; Girardi et al. 1996); the model atmospheres compiled by Lejeune, Cuisinier, & Buser (1997, 1998), as corrected by Westera (2001) and Westera et al. (2002); and the IMF parameterized by Chabrier (2003), truncated at  $0.1 M_\odot$  and  $100 M_\odot$ . Our choice of the “standard” models is based on the assessment of Bruzual & Charlot (2003), and on tests that we

made specifically with the MC cluster data as well.

We compute SBF and integrated magnitudes and colors, through the 2MASS near-IR filters, of single-burst stellar populations for ages of 1 Myr – 17 Gyr and metallicities  $Z = 0.0004 - 0.05$ .

First of all, we have used the models to check that, in fact, the stars that are detected as point sources by the 2MASS survey are enough to obtain a reliable estimate of the near-IR SBFs of the Magellanic star clusters. Fig. 4 shows, for  $Z = 0.0004, 0.004, 0.008$ , and  $0.05$ , the difference between the  $J$ ,  $H$ , and  $K_s$  integrated and fluctuation magnitudes calculated with all the stars and only from those with  $M_{K_s} \leq -4.5$  (or  $K_s = 14$  at the LMC).<sup>12</sup> This difference is actually an overestimate, since we do detect fainter stars. Excepting extremely young ages that are not relevant to this work, even when the contribution from the bright stars to the integrated luminosity is of the order of 10–20 percent, at an age of half to 1 Gyr, depending on metallicity —when supergiants have died and giants are yet to appear—, or at  $\sim 10$  Gyr —when the luminosity of the RGB dwindles (see §6)—, the foreseen differences in the derived fluctuation magnitudes are always smaller than the expected empirical errors due to stochastic fluctuations in the number of stars (cf. Fig. 4 and Table 4), as we discuss here below. As an additional check, Table 5 compares, for all eight superclusters, the theoretical and measured contributions from stars with  $M_{K_s} \leq -4.5$  to the *integrated*  $J$ ,  $H$ , and  $K_s$  fluxes. There is quite a good agreement, except for the intermediate age superclusters classes III and IV, where the models underestimate the light fraction from bright stars by a factor of  $\sim 2$ .<sup>13</sup> The actual minimum contributions of  $\sim 20\%$  are observed for class VII (remarkably, exactly at the levels anticipated by the models); these minimal ratios would translate into discrepancies in the SBFs that would increase the errors quoted in Table 4 by a few hundredths of a magnitude only.

#### 4.1. Stochastic errors

Stochastic errors due to small number statistics are central to SBF studies of star clusters. The standard way to assign error bars to fluctuation magnitudes and colors has so far been through Monte Carlo simulations (e.g., Ajhar & Tonry 1994; Bruzual 2002). Recently, however, Cerviño et al. (2002) have presented an approximate statistical formalism to estimate quantitatively the dispersion expected in relevant observables of simple stellar populations, owing to statistical fluctuations of the luminosity function. This approach is based on the assumption that the variables involved have a Poissonian nature; it shows explicitly that models can be used to accurately predict the scatter observed in real data, if the theoretical relative error produced by stochastic fluctuations

---

<sup>12</sup>In order to obtain the fluctuation magnitudes, the second moments derived from the bright stars are still normalized by the integrated luminosity of all the stars, as is done with the data.

<sup>13</sup>Although models with higher metallicity also predict a larger contribution from bright stars, even models with  $Z = 0.05$  cannot match the data.

in the number of stars is scaled by  $M_{tot}^{-1/2}$ , where  $M_{tot}$  is the total mass of the stellar population. An important ingredient when calculating the dispersion in this fashion are the covariance terms. The covariance between two quantities,  $\text{cov}(x, y)$ , is defined as

$$\text{cov}(x, y) = \rho(x, y)\sigma_x\sigma_y, \quad (4)$$

where  $\rho(x, y)$  is the correlation coefficient and  $\sigma_x$  and  $\sigma_y$  are, respectively, the uncertainties due to small number statistics in  $x$  and  $y$ .  $\rho(x, y)$  varies between -1 and 1, depending on the sign of the correlation: a positive correlation means that the quantities vary together in the same direction; a negative correlation occurs when the quantities vary together in opposite directions (in this work, we will denote with a minus sign a covariance with a negative correlation coefficient). If  $\rho(x, y) = 0$ , the quantities are not correlated, i.e., they are statistically independent. For one given star, for example, the luminosities in different bands are completely correlated. For a group of stars, though, the contribution from each star has to be considered for a proper calculation of the covariance. In general, in the case of observables —like integrated colors and surface brightness fluctuations of stellar populations— that are ratios of luminosities, the adoption *a priori* of  $\rho = 0$  will overestimate the error.

Cerviño et al. (2002) verify that their method works for integrated properties, such as colors and equivalent widths of emission and absorption lines, through cross-checks with the outcome of, again, Monte Carlo simulations. Here, we apply the method of Cerviño et al. (2002) to derive error bars for integrated magnitudes, integrated colors, fluctuation magnitudes, and fluctuation colors. The operations performed in each case are presented in Appendix A. Through new comparisons with Monte Carlo simulations, we have corroborated that the chosen approach is applicable to fluctuation magnitudes and colors as well. For cluster masses higher than a few  $\times 10^5 M_\odot$ , our “analytical” error bars and the Monte Carlo errors are equivalent, although one must bear in mind that these analytical errors are  $1-\sigma$ , whereas Monte Carlo simulations will generate results within  $3-\sigma$  of the “central” analytical value.<sup>14</sup>

Furthermore, we have calculated errors not just from the models, but also directly from the data. When working with the models, all equations are applied as written down in the appendix; there,  $w_i$  stands for the number of stars of mass  $m_i$  by unit mass, and  $M$  is in each case the mass of the supercluster in question. The supercluster masses are obtained from the models themselves, using the theoretical near-IR mass-to-light ratios of a population with the same age and metallicity as each supercluster; the tabulated errors in the masses in Tables 3 and 4 are equal to the dispersion

<sup>14</sup>For lower cluster masses, sampling fluctuations will produce biases (i.e., deviations from the theoretically predicted values of the observables) and multimodality that depend on wavelength and stellar evolutionary phase, and that cannot be accounted for by our analytical calculation of the stochastic errors (Santos & Frogel 1997; Cantiello et al. 2003; Cerviño & Valls-Gabaud 2003; Raimondo et al. 2003). Investigating these effects is beyond the scope of this paper.

of the results at  $J$ ,  $H$ , and  $K_s$ .<sup>15</sup> When dealing with data, however, we perform sums over individual stars; hence, all the  $w_i$ 's are assumed to be unity. Also, in the case of the data, it is unnecessary to normalize by  $M^{-1/2}$ , since this operation is implicitly done by adding the stars. Typically, the errors derived from the data —which are the ones we quote— are about 2–3 times the size of the error bars anticipated from the models.<sup>16</sup>

Yet another check has been provided by the comparison between our errors and those quoted by Liu, Graham, & Charlot (2002) for  $\bar{K}_s$  and  $(V - I_c)$  of Fornax Cluster galaxies. The errors in the present paper are about twice larger, for both integrated and fluctuation magnitudes. Since the Fornax Cluster elliptical and S0 galaxies analyzed are 3–4 orders of magnitude more massive than our superclusters,<sup>17</sup> and given that relative errors scale as  $M^{-1/2}$ , it follows that the stochastic effects are about 30 times smaller for the Fornax galaxies, and hence a negligible contributor to the error budget of their derived SBFs. This budget includes contributions from distance errors, the depth of the Fornax cluster and, necessarily, the composite nature of the stellar populations of the galaxies.

Incidentally, we have calculated approximately the (unknown) correlation coefficients  $\rho(a, b)$  for model integrated and fluctuation near-IR colors, assuming that the colors have the form  $u = a/b$ , where

$$\frac{\sigma_u^2}{u^2} = \frac{\sigma_a^2}{a^2} + \frac{\sigma_b^2}{b^2} - 2 \frac{\text{cov}(a, b)}{ab}. \quad (5)$$

A comparison between the results obtained with the appropriate “exact” calculation in Appendix A, and the “naïve” formula above yields  $\rho(a, b)$ . We find that, for all metallicities, the coefficients  $\rho(a, b)$  for fluctuation colors are  $\sim -1$  at all ages, while those for integrated colors are  $\sim -0.9$  in the case of a very young population, but reach  $\sim -0.98$  after about 3.5 Myr.

## 4.2. Systematic errors

Aside from the problem posed by small number statistics, two other issues are crucial for SBF measurements of star clusters, in view of the way they are performed: the sky level, which

<sup>15</sup>The supercluster mass increases with age; this is probably just a manifestation that more massive clusters are more resilient against disruption and survive longer.

<sup>16</sup>Exceptionally, the data errors for the youngest (Pre-SWB) supercluster are  $\sim$  one order of magnitude larger than those predicted by the models. In this case, the mass of the supercluster could have been overestimated; it probably is no coincidence that this is the mass determination with the largest (absolute and relative) error (see Tables 3 and 4).

<sup>17</sup>From their line-of-sight velocity dispersions (Hypercat, <http://www-obs.univ-lyon1.fr/hypercat>, which uses an updated version of the literature compilation by Prugniel & Simien (1996); Graham et al. (1998)) and assuming a mass-to-light ratio of  $\sim 2$  (Faber & Jackson 1976), the galaxies have masses  $\leq 10^9 M_\odot$ .

impacts the denominator of equation 3, and crowding which, through the blending of sources, will in principle make the numerator larger and hence the SBF magnitude brighter. We invite the reader here to inspect the top left panel of Figure 5, where we present the  $H$ -band absolute fluctuation magnitude vs age of the eight MC superclusters, carried out as we have described in §3. Models of different metallicities, that will be discussed in detail in §5.2, are also plotted. The color-coded dots are measurements obtained from different regions of the superclusters: the central  $0''$  to  $20''$  (red), the annulus between  $20''$  to  $40''$  (blue), and the annulus between  $40''$  to  $60''$  (green); the black dots are the values derived from the analysis of the whole region within  $1'$  of the center of the superclusters. The central red dots should be most affected by crowding, while the outside green dots should be most sensitive to over or undersubtraction of sky emission.

First, we notice the paradoxical result that, with the exception of the youngest Pre-SWB supercluster, the red dots are fainter than the rest, instead of brighter. While the centralmost region of the Pre-SWB supercluster shows the expected bias, the remaining superclusters display an indirect effect of crowding, by virtue of which blended sources appear (rather than brighter) as suffering from bad photometric measurements, and hence are discarded. The green dots derived from the outermost annuli, on the other hand (and again with the exception of the Pre-SWB supercluster), tend to appear a little too bright, presumably as a consequence of sky emission oversubtraction. However, excepting the central regions of classes V and VI, the results for all the regions of all the clusters are consistent with each other. Moreover, on the question of crowding, Ajhar & Tonry (1994) discarded for this reason regions of their data where the two brightest magnitudes covered more than 2% of the area. We have inspected the luminosity functions of the individual MC star clusters (including all sources in the PSC, regardless of photometric quality) and found that, while the regions within  $20''$  of the centers of most of them would be deemed crowded by this criterion, already the regions within  $40''$  of the centers, taken as a whole, would not. Consequently, we will adopt the measurements from the circular regions within  $1'$  of the center of the superclusters, given that they seem to provide the better balance of uncertainties owing to crowding and sky subtraction, and that (unlike the annuli between  $20''$  and  $40''$ ) they should also be the least affected by small number statistics.

The middle left panel of Figure 5 shows the  $(\bar{H} - \bar{K}_s)$  fluctuation color vs age for the MC superclusters. Measurements obtained from different regions are color-coded as before. Although the relative position of the different values obtained for each cluster are harder to interpret in terms of crowding or faulty subtraction of sky emission, we find again that all the results are consistent within the Poisson error bars.

We show in the bottom left panel of Figure 5 the ratio of the observed and model contributions of stars brighter than  $M_{K_s} = -4.5$  to integrated light at  $H$ . Here we see once more that blended stars have been preferentially thrown out in central regions, while outermost annuli are very sensitive to sky emission subtraction. For superclusters I, II, V, VI, and VII, not only the match between models and data within  $1'$  of their centers is good, but the color points scatter around 1. However, for superclusters Pre, III, and IV, all points lie above unity. Especially in the case of classes III and

IV, this is likely pointing to a lack of theoretical understanding of AGB stars and their contribution to the integrated light of the clusters, rather than caused by problems with the data and their treatment.

For completeness, in the right panels of Figure 5 we present the same measurements, but now including the fluxes from all point sources, irrespective of their photometric quality. The agreement with the models is of the same order as before and, if drawn from these results, our conclusions would hold.

### 4.3. Other errors

We have assumed that the photometric error in the integrated luminosity of each individual cluster frame is at most 10%, or the 2MASS survey specification for galaxy photometry.<sup>18</sup> Given that between 12 and 35 individual clusters have been combined to construct each supercluster (Tables 3 and 4), added in quadrature these errors would translate into a photometric uncertainty of 0.02 – 0.03 mag in the integrated luminosity of the superclusters, at which point we should be hitting systematic effects. The photometric errors of the fluctuation luminosities and colors have contributions from both the integrated and the point source photometry. However, in view of the errors in the point source photometry quoted by the 2MASS PSC, the total photometric errors are dominated by the aforementioned uncertainty in the integrated luminosity. Accordingly, and hopefully conservatively, we adopt a photometric error of 0.03 mag in the superclusters’ integrated luminosities, integrated colors, fluctuation luminosities and fluctuation colors, which we add in quadrature to the stochastic errors discussed above in section §4.

In the case of Fornax Cluster galaxies, errors for  $\bar{K}_s$  fluctuation magnitudes are taken from Liu, Graham, & Charlot (2002), and those for  $\bar{H}$  come from Jensen et al. (2003). The uncertainties in their fluctuation colors are computed assuming a correlation coefficient  $\rho$  of -0.9. Errors in integrated colors of galaxies are calculated from the uncertainties in their integrated fluxes quoted by the 2MASS Extended Source Catalog, also with  $\rho = -0.9$ . The uncertainties in the galaxy ages and abundances, [Fe/H] (transformed to errors in metallicity, Z), are averages taken from Figure 12 in Kuntschner (2000); they both have the value of  $\pm 0.15$  dex. Finally, for the clusters and after Cohen (1982), we take errors of  $\pm 0.2$  dex in abundance, and uncertainties in their ages of  $\pm 0.3$  dex.

## 5. Results

Our measurements of MC superclusters are summarized in Tables 3 and 4. There we give, respectively, cluster integrated and fluctuation magnitudes and colors. The results proper are

---

<sup>18</sup><http://pegasus.phast.umass.edu/2MASS/teaminfo/level1.ps>

presented in Figures 6 through 12.

### 5.1. Integrated colors vs age

In order to put the SBF measurements in context, we begin by plotting in Figure 6 the integrated colors vs log (age). The left panels overplot the Fornax and MC data points with the models, while the right panels display the data points with error bars. Models redden with age, first as massive stars become red supergiants, then as the AGB is populated by intermediate mass stars, and finally as the brighter stars in the populations are low mass stars in the RGB and AGB. After  $10^7$  years, models of the same age with higher metallicities are redder, owing to increased opacity, which causes the stellar atmospheres to expand and cool. For stars with  $T_{eff} \approx 3000 - 6000$  K, the main source of opacity are the H<sup>-</sup> ions, for which metals with low-ionization potential are the principal electron donors; in addition, opacity from lines and molecular bands (depending on stellar temperature) also increases with higher metallicity.

Focusing on the data, we notice that the Pre-SWB supercluster is noticeably redder than the models in all three colors,  $\Delta(J - H)$  and  $\Delta(H - K_s) \sim 0.4$ . This is probably due mainly to the fact that the age we have assumed for the supercluster is only an average —the supercluster includes objects from  $10^6$  to almost  $10^7$  years old—, and at this point in their evolution clusters redden rapidly as they age. Dust reddening might also have a (very small) role, since younger clusters suffer on average from 3 times more extinction than older ones (Charlot & Fall 2000). The extreme discrepancy between bluer models and redder clusters decreases gradually through class I and all but disappears by class II, at a few  $\times 10^7$  years. According to the models, for objects older than a few  $\times 10^8$  years it is hard to use integrated colors to discriminate between metal-rich and metal-poor objects. However, the two oldest superclusters, classes VI and VII, fall exactly in the loci predicted by the models given their metallicities.

### 5.2. Fluctuation magnitudes vs age

We get a remarkable general agreement between models and data, including the Fornax Cluster galaxies, when we look at fluctuation magnitude vs log (age), Fig. 7. Models show the fluctuations getting brighter between 1 and 10 Myr, and progressively fainter after that. For  $\bar{M}(H)$  and especially for  $\bar{M}(K_s)$ , after  $10^8$  years models with higher metallicity are brighter at a fixed age (while for  $\bar{M}(J)$ , at ages older than 1 Gyr, the models are quite insensitive to metallicity). This is mostly an effect of what we have discussed earlier: more metal rich populations are redder and, therefore, brighter in the near-IR. For example, the  $K$ -band magnitude of the tip of the RGB (TRGB) of Milky Way clusters rises monotonically with metallicity, and is roughly one magnitude brighter at  $[Fe/H] \sim -0.2$  than at  $[Fe/H] \sim -2.2$  (Ferraro et al. 2000).

The data follow the trend delineated by the models, except that the behavior of the data

between 1 and 50 Myr is less conspicuous than the theoretical one, owing mainly to the fact that the point for the SWB I supercluster is slightly fainter than foreseen by the models. The brightness decline at the oldest ages is intensified by the fact that the two oldest superclusters are of progressively lower metallicities.

The extreme and short-lived brightening of the fluctuation magnitude between  $10^6$  and  $10^7$  years is powered by red supergiants, while fluctuations of intermediate-age populations (500 Myr to 1 Gyr old) are fueled by intermediate mass stars in the AGB, which are brighter and redder than the TRGB (e.g. Frogel, Persson, & Cohen 1980). For older populations, the fluctuations are driven by low mass stars in the RGB and AGB; the AGB is slightly bluer but not brighter than the RGB at those stages. The gradual dimming of the fluctuation magnitude with age after 1 Gyr is a result of the reduction of the RGB average brightness. This goes down, even though the luminosity of the TRGB stays constant and the IMF is rising, because lower mass stars evolve at slower rates (Iben 1967), and therefore spend longer and longer times at lower luminosities in the RGB. We illustrate these points with Figure 8. It shows the evolution of the TRGB  $K_s$  magnitude, the average RGB  $K_s$  magnitude, and the  $K_s$  magnitude of the mode of the RGB luminosity function, for a population with  $Z = 0.0004$ . All magnitudes are in an arbitrary scale, and they are plotted vs main-sequence turn-off (MSTO) mass and log (age). Between 400 Myr and  $\sim 1$  Gyr all functions first decrease, then increase in brightness. But after 1.5 Gyr the TRGB luminosity stays roughly constant, fueled by core helium ignition, while the average RGB brightness decreases steadily. As a consequence too of the onset of core degeneracy—which means that energy is now furnished by H-shell burning only—the brightness of the mode of the RGB luminosity function plummets at 1 Gyr, and subsequently dwindle with the progressively smaller MSTO.

### 5.3. Fluctuation colors vs age

We display next plots of fluctuation color vs the logarithm of the age (Fig. 9).<sup>19</sup> First focusing on the models in the top panels, we see that, like those for integrated colors, those with higher metallicities are redder. However, rather than just reddening with age, they get redder until they reach a maximum, at  $\sim 500$  Myr; afterwards, those with metallicities of  $Z = 0.008$  and higher become slightly bluer as the RGB takes over, but then roughly keep a constant color, while the models with  $Z = 0.004$  and lower turn bluer progressively thereafter. The reddest point at each metallicity is due to the cool, bright, AGB populated by intermediate-mass stars in intermediate-age systems.

The behavior of the fluctuation color with age after  $\sim 1$  Gyr, for different metallicities, is a result of several features of the RGB morphology: (1) we have already mentioned here that, for a

---

<sup>19</sup>The models with age =  $10^6$  yr are too blue and fall off the scale in  $(\bar{J} - \bar{H})$  and  $(\bar{J} - \bar{K}_s)$ . On the other hand, the model with  $5 \times 10^8$  yr and  $Z = 0.008$  is too red in  $(\bar{J} - \bar{H})$ .

single age, the RGB temperature is lower for higher metallicities; (2) for a single metallicity, the temperature of the RGB diminishes with age (Iben 1967; VandenBerg & Bell 1985); (3) the amount of this difference in temperature between populations of different ages is a function of metallicity and in general is larger for higher Z (VandenBerg & Bell 1985; Rood & Crocker 1997); (4) the RGB is sloped, in the sense that more luminous stars are cooler than fainter ones, and the difference in temperature between bright and faint stars increases with metallicity (e.g., Kuchinski & Frogel 1995; Ferraro et al. 2000).<sup>20</sup>

Figure 10 shows how these features interplay with the fact —discussed above in §5.2— that the RGB has a fainter average luminosity as a population ages, in order to determine the evolution of RGB color (and fluctuation color) with time, at several metallicities. In this figure, we plot the average  $K_s$  magnitude (arbitrary units) vs the average  $(J - K_s)$  integrated color of the RGB plus AGB, for populations with  $Z=0.004$ ,  $Z=0.008$ , and  $Z=0.05$ . The color is followed between 400 Myr (top of lines) and 20 Gyr (bottom of lines). In the case of the models we have used, the maximum temperature difference of the RGB with age occurs at  $Z = 0.008$ . We see that the RGB plus AGB color of the  $Z = 0.004$  model grows significantly bluer after 400 Myr and, despite reddening later, is still bluer at 20 Gyr than at 400 Myr; the color reddens almost constantly for  $Z = 0.008$ ; and it stays barely constant with time for  $Z = 0.05$ . Hence, for  $Z = 0.004$ , the contribution from fainter, hotter stars wins over the difference in temperature of the RGB due to age, and over the smaller slope; the difference in temperature with age is dominant, even with a steeper slope, for  $Z = 0.008$ ; and all three effects compensate each other to yield a roughly constant temperature as the population evolves for  $Z=0.05$ . The progression of the RGB plus AGB integrated color seen in this graph is mirrored (albeit in an exaggerated fashion) by the model fluctuation colors in Figure 9.

The behavior of our mixed metallicity star cluster data, on the other hand, is much smoother than the models. This is not surprising, given the widths of our observed RGBs (Fig. 3). The agreement between data and models is closer for  $(\bar{H} - \bar{K}_s)$ , but in all three fluctuation colors the data do not show a maximum. Instead, we can almost distinguish two groups: the superclusters with  $\log(\text{age}/\text{yr}) < 8$ , where massive main-sequence stars and red supergiants power the SBFs, and those with  $\log(\text{age}/\text{yr}) > 9$ , where fluctuations are produced by low-mass stars in the RGB and

---

<sup>20</sup>Most of these characteristics are related to H<sup>-</sup> opacity, which in turn is connected to metallicity, and to the dependence of ionization fraction on both atmospheric temperature and density (Renzini 2003). The RGB temperature diminishes with age because, since core mass in this evolutionary phase is roughly independent from stellar main-sequence mass, a lower MSTO mass means a less massive atmosphere with less pressure which, consequently, expands and cools more. The size of the RGB temperature difference with age depends on opacity. Initially, more metals will produce more continuum opacity, and hence more atmospheric expansion and lower temperature; a lower density will further increase the ionization fraction and the opacity. However, a point will be reached when the low temperature will cause the ionization fraction and the opacity to diminish. The RGB slope can be explained along similar lines: the ascent upwards the RGB is caused by atmospheric expansion. This expansion increases the stellar luminosity, but also decreases the density of the atmosphere. With lower density, the ionization fraction and the opacity increase, with the subsequent diminution in temperature. The effect is stronger, and therefore the slope is larger, for higher metallicity.

AGB. There is an isolated point in these panels: the SWB III supercluster,  $5 \times 10^8$  years old, where red giants with intermediate mass progenitors must be driving the SBFs; the coolest AGB stars that in theory dominate intermediate-age populations in the near-IR do not manifest themselves in the fluctuation colors of these data. Finally, even though we do see the bluer color at older ages that can be explained by the progressively lower metallicities of superclusters VI and VII, the data overall display a tendency to redden with age that can be fit by a straight line.

Thus, we find, *for the superclusters only*:

$$(\bar{J} - \bar{H}) = (0.10 \pm 0.02)\log(\text{age}/\text{yr}) + (0.29 \pm 0.19) \quad (6)$$

$$(\bar{H} - \bar{K}_s) = (0.21 \pm 0.03)\log(\text{age}/\text{yr}) - (1.29 \pm 0.22) \quad (7)$$

$$(\bar{J} - \bar{K}_s) = (0.30 \pm 0.04)\log(\text{age}/\text{yr}) - (0.97 \pm 0.36). \quad (8)$$

About one third of the galaxies, on the other hand, fall at a redder ( $\bar{H} - \bar{K}_s$ ) color than the superclusters and all of the models. If, this notwithstanding, we include them in the linear fit, we get

$$(\bar{H} - \bar{K}_s) = (0.20 \pm 0.02)\log(\text{age}/\text{yr}) - (1.25 \pm 0.16). \quad (9)$$

Table 6 lists the coefficients of these fits. The reduced chi-square ( $\tilde{\chi}^2$ ) and the rms of the points (in magnitudes) after the fits are also included.

#### 5.4. Trends with metallicity

For completeness, we present plots of fluctuation magnitudes and colors vs metallicity. On average, populations with higher metallicities are brighter and redder at the same age, but the behavior followed by the models here can be understood in more detail from our exposition of RGB and AGB brightnesses and colors in the subsections above.

Fig. 11 displays the  $\bar{J}$ ,  $\bar{K}_s$ , and  $\bar{H}$  fluctuation magnitudes vs metallicity. Here, the match between models and data is in general good. The data points for the MC superclusters, in the low metallicity (left) region of the plots, show once more a general trend with age, where younger populations are brighter than older ones —although in particular supercluster Pre-SWB is much brighter than the models, and superclusters classes V, VI, and VII are somewhat brighter than the models. The Fornax Cluster galaxies, on the other hand, clump up in the high metallicity (right) regions of the middle and bottom panels, where models 2 Gyr and older “funnel” and loose the ability to make fine distinctions in age.

In Fig. 12, we plot the  $(\bar{H} - \bar{K}_s)$  fluctuation color vs metallicity. In order to facilitate the comparison with the models, the top panels show the MC clusters only, while the bottom ones include the Fornax galaxies also. The Pre-SWB supercluster is redder than the models, while classes III, VI and VII are somewhat bluer, but data and models mirror each other in the tendency for objects up to 5 Gyr to redden with age; the two oldest superclusters then become bluer, owing both to age (see §5.3) and their lower metallicities. On the other hand, a few of the Fornax galaxies seem significantly redder than the reddest models, and indeed the galaxy average, although matching the models between 500 Myr and 2 Gyr, is only marginally consistent with those between 5 and 17 Gyr old. (We remind the reader that the error bars of the galaxy fluctuation color have been calculated using information from the literature and assuming a correlation coefficient of -0.9 between any two given passbands, while errors for SBFs of the MC superclusters have been derived directly from the data.)

## 6. Conclusions and Future Work

This study has shown that in MC star clusters, most of which have roughly the same relatively low metallicity, near-IR fluctuation magnitudes and colors are driven by age.

Our result is not unexpected. In their classical study, Searle, Wilkinson, & Bagnuolo (1980) demonstrated that the properties of the MC clusters' integrated light *in the optical wavelengths* are determined by their red giants. They also inferred that the sequence from class I to class III is one of age, and insensitive to abundance. Regarding the sequence of the older clusters, classes IV through VII, Searle, Wilkinson, & Bagnuolo (1980) posited that it was both sensitive to increasing age *and* decreasing metallicity. Given that (a) both near-IR wavelengths and SBFs are more sensitive than integrated optical light to the red giant stars in these clusters, and (b) the star cluster metallicity stays nearly the same for classes Pre through V, it is not surprising that we have also found a sequence of age, slightly modulated by abundance in the case of the two oldest SWB classes.

It is true that the MC star clusters are mostly either too young (7 out of the 8 MC superclusters are younger than most of the Fornax galaxies) and/or too metal-poor to be relevant to the galaxies. However they seem to outline a trend with age that includes the galaxies, as is shown most clearly by Figure 7. For this reason, even if star cluster populations might be of limited direct value for the modelling of old ellipticals and spheroids, they are important for the calibration of stellar population synthesis models.

Regarding the agreement between the data and the models in their present state, we find that it is very good qualitatively, but that it could be improved in the details. For example, in principle, we could have read off the metallicity of the superclusters from Figures 7 and 9, given their ages. However, the metallicities we would have inferred are not consistent in all cases with the ones that correspond to their SWB class. Also, the models, and in particular those with the highest metallicity, cannot reproduce the very red fluctuation colors exhibited by a few of the

Fornax galaxies. Conversely, models predict redder fluctuation colors than those of intermediate-age clusters, and they underestimate the contribution of bright stars to the integrated luminosity in these same clusters. Arguably, the models work best for old, metal poor populations. This is probably not a coincidence, but is due to the fact that models have tried to match their features for the longest time. Moreover, old populations evolve more slowly. On the MC supercluster data side, the oldest clusters are also the most massive, and therefore have the smallest stochastic errors. The rapidly evolving young populations are harder to match, as are the intermediate-age ones, with their poorly, albeit increasingly better, understood asymptotic giant branches.

We plan to continue this work in various directions, e.g., improve the calibration of the models with the SBF data, compare to other models, and compute SBFs of the highest metallicity clusters in our Galaxy and in M 31. We will also investigate the relationship between  $\bar{M}_{K_s}$  and  $(V - I)$  color in the MC star clusters. Liu, Graham, & Charlot (2002) discovered a linear dependence of  $\bar{M}_{K_s}$  with  $(V - I)$  in a sample of 26 ellipticals, S0s, and spiral bulges, which might be tracing late bursts of star formation in these systems; a study of the MC star clusters, which probe a range twice as large in  $\bar{M}_{K_s}$  and three times larger in color, is likely to throw light into the origin of this trend.

This research has made use of the VizieR Service and the SIMBAD database at the Centre de Données Astronomiques de Strasbourg, as well as NASA’s Astrophysics Data System Abstract Service. R.A.G. acknowledges support from two Mexican organizations, respectively, the National Researcher System (SNI) and the National Council of Science and Technology, CONACyT (grant 36042-E); she also thanks A. Watson for suggesting the use of the 2MASS database, P. D’Alessio for her help with plotting macros, M. Cerviño for lively discussions regarding errors, S. Van Dyk for dissipating doubts about the 2MASS survey, and L. Loinard for his willingness to discuss every aspect of this work. M.C.L. is grateful to research support from NASA grant HST-HF-01152.01-A. GBA acknowledges support from the Venezuelan Ministerio de Ciencia y Tecnología and FONACIT. We express our appreciation to the anonymous referee, whose pertinent and helpful suggestions allowed us to improve the robustness of our results. It is our pleasure to thank James R. Graham for inspiring this work.

## A. Error propagation

Following Buzzoni (1989) and Cerviño et al. (2002), one can estimate the relative error, in the Poissonian limit, for any synthesized quantity  $A$  which is the sum of the contributions from individual stars (or populations); i.e.,  $A = \sum w_i a_i$ , where  $a_i$  is the contribution of the  $i^{th}$  star (or stellar type), and  $w_i = N_i/M_{tot}$  is the mean value of the number of stars of mass  $m_i$ , normalized to the total mass of the cluster  $M_{tot} = \sum m_i$  (assumed to be a constant).  $w_i$  is treated as a random variable, but  $a_i$  is considered a fixed quantity; in this case,

$$\sigma_A^2 = \sum a_i^2 \sigma_{w_i}^2. \quad (\text{A1})$$

Now,

$$\sigma_{w_i}^2 = \frac{N_i}{M_{tot}^2} = \frac{w_i}{M_{tot}}, \quad (\text{A2})$$

so that the relative error is

$$\frac{\sigma_A}{A} = \frac{\left(\frac{1}{M_{tot}} \sum w_i a_i^2\right)^{1/2}}{\sum w_i a_i}. \quad (\text{A3})$$

Notice that the importance of the stochastic fluctuations in the number of contributing stars goes down as the total mass of the cluster increases.

### A.1. Error of an integrated monochromatic luminosity.

In this case, Eq. A3 applies directly. Suppose that  $J$  is the integrated luminosity in the  $J$ -band and  $j_i$  is the contribution from the  $i^{th}$  stellar type; then

$$\frac{\sigma_J}{J} = \frac{\left(\frac{1}{M_{tot}} \sum w_i j_i^2\right)^{1/2}}{\sum w_i j_i}. \quad (\text{A4})$$

The error in magnitudes is the relative error  $\times 2.5 \times \log_{10}(e)$ , or

$$1.0857 \times \frac{\sigma_J}{J} \text{ mag} \quad (\text{A5})$$

### A.2. Error of an integrated color.

We begin by expressing the color as the ratio of two luminosities, or

$$c = \frac{\sum w_i a_i}{\sum w_i b_i} \equiv \frac{u}{v}; \quad (\text{A6})$$

$a_i$  and  $b_i$  are, respectively, the contributions of stars of type  $i$  in each wavelength. In this case, the fluxes in the two bands *are* correlated, but we assume that  $w_i$  is independent from both  $a_i$  and  $b_i$ . We will apply the following equation for the relative error of a random variable  $z = x/y$ :

$$\frac{\sigma_z^2}{z^2} \simeq \frac{\sigma_x^2}{x^2} + \frac{\sigma_y^2}{y^2} - 2 \frac{\text{cov}(x, y)}{xy}. \quad (\text{A7})$$

So,

$$\sigma_u^2 = \frac{1}{M_{tot}} \sum w_i a_i^2 \quad (\text{A8})$$

$$\sigma_v^2 = \frac{1}{M_{tot}} \sum w_i b_i^2 \quad (\text{A9})$$

$$\text{cov}(u, v) = \frac{1}{M_{tot}} \sum w_i a_i b_i. \quad (\text{A10})$$

Hence, the relative error square is

$$\frac{\sigma_c^2}{c^2} \simeq \frac{\frac{1}{M_{tot}} \sum w_i a_i^2}{(\sum w_i a_i)^2} + \frac{\frac{1}{M_{tot}} \sum w_i b_i^2}{(\sum w_i b_i)^2} - \frac{\frac{2}{M_{tot}} \sum w_i a_i b_i}{\sum w_i a_i \sum w_i b_i}, \quad (\text{A11})$$

and the relative error in magnitudes is

$$1.0857 \times \left( \frac{\sigma_c^2}{c^2} \right)^{1/2} \text{ mag} \quad (\text{A12})$$

### A.3. Error of a fluctuation luminosity.

This is again the case of a ratio:

$$\bar{l} = \frac{\sum w_i a_i^2}{\sum w_i a_i} \equiv \frac{u}{v}; \quad (\text{A13})$$

$a_i$  and  $a_i^2$  are, of course, correlated. So,

$$\sigma_u^2 = \frac{1}{M_{tot}} \sum w_i a_i^4 \quad (\text{A14})$$

$$\sigma_v^2 = \frac{1}{M_{tot}} \sum w_i a_i^2 \quad (\text{A15})$$

$$\text{cov}(u, v) = \frac{1}{M_{tot}} \sum w_i a_i^3, \quad (\text{A16})$$

and

$$\frac{\sigma_l^2}{l^2} \simeq \frac{\frac{1}{M_{tot}} \sum w_i a_i^4}{(\sum w_i a_i^2)^2} + \frac{\frac{1}{M_{tot}} \sum w_i a_i^2}{(\sum w_i a_i)^2} - \frac{\frac{2}{M_{tot}} \sum w_i a_i^3}{\sum w_i a_i^2 \sum w_i a_i}; \quad (\text{A17})$$

the relative error in magnitudes is

$$1.0857 \times \left( \frac{\sigma_l^2}{l^2} \right)^{1/2} \text{ mag} \quad (\text{A18})$$

#### A.4. Error of a fluctuation color.

We express the fluctuation color as follows:

$$fc = \frac{\sum w_i a_i^2 / \sum w_i a_i}{\sum w_i b_i^2 / \sum w_i b_i} = \frac{\sum w_i b_i}{\sum w_i a_i} \cdot \frac{\sum w_i a_i^2}{\sum w_i b_i^2} \equiv \frac{u}{v} \cdot \frac{r}{s}; \quad (\text{A19})$$

since  $a_i$ ,  $a_i^2$ ,  $b_i$ , and  $b_i^2$  are all correlated,

$$\begin{aligned} \frac{\sigma_{fc}^2}{(fc)^2} &\simeq \frac{\sigma_u^2}{u^2} + \frac{\sigma_r^2}{r^2} + 2\frac{\text{cov}(u, r)}{ur} + \frac{\sigma_v^2}{v^2} + \frac{\sigma_s^2}{s^2} + 2\frac{\text{cov}(v, s)}{vs} \\ &\quad - 2\frac{\text{cov}(u, v)}{uv} - 2\frac{\text{cov}(r, v)}{rv} - 2\frac{\text{cov}(u, s)}{us} - 2\frac{\text{cov}(r, s)}{rs} \end{aligned} \quad (\text{A20})$$

$$\sigma_u^2 = \frac{1}{M_{tot}} \sum w_i b_i^2 \quad (\text{A21})$$

$$\sigma_r^2 = \frac{1}{M_{tot}} \sum w_i a_i^4 \quad (\text{A22})$$

$$\sigma_v^2 = \frac{1}{M_{tot}} \sum w_i a_i^2 \quad (\text{A23})$$

$$\sigma_s^2 = \frac{1}{M_{tot}} \sum w_i b_i^4 \quad (\text{A24})$$

$$\text{cov}(u, r) = \frac{1}{M_{tot}} \sum w_i a_i^2 b_i \quad (\text{A25})$$

$$\text{cov}(v, s) = \frac{1}{M_{tot}} \sum w_i a_i b_i^2 \quad (\text{A26})$$

$$\text{cov}(u, v) = \frac{1}{M_{tot}} \sum w_i a_i b_i \quad (\text{A27})$$

$$\text{cov}(r, v) = \frac{1}{M_{tot}} \sum w_i a_i^3 \quad (\text{A28})$$

$$\text{cov}(u, s) = \frac{1}{M_{tot}} \sum w_i b_i^3 \quad (\text{A29})$$

$$\text{cov}(r, s) = \frac{1}{M_{tot}} \sum w_i a_i^2 b_i^2 \quad (\text{A30})$$

Therefore,

$$\begin{aligned} M_{tot} \cdot \frac{\sigma_{fc}^2}{(fc)^2} &\simeq \frac{\sum w_i b_i^2}{(\sum w_i b_i)^2} + \frac{\sum w_i a_i^4}{(\sum w_i a_i^2)^2} + 2 \frac{\sum w_i a_i^2 b_i}{\sum w_i a_i^2 \sum w_i b_i} \\ &+ \frac{\sum w_i a_i^2}{(\sum w_i a_i)^2} + \frac{\sum w_i b_i^4}{(\sum w_i b_i^2)^2} + 2 \frac{\sum w_i a_i b_i^2}{\sum w_i a_i \sum w_i b_i^2} \\ &- 2 \frac{\sum w_i a_i b_i}{\sum w_i a_i \sum w_i b_i} - 2 \frac{\sum w_i a_i^3}{\sum w_i a_i \sum w_i a_i^2} \\ &- 2 \frac{\sum w_i b_i^3}{\sum w_i b_i \sum w_i b_i^2} - 2 \frac{\sum w_i a_i^2 b_i^2}{\sum w_i a_i^2 \sum w_i b_i^2} \end{aligned} \quad (\text{A31})$$

and the relative error in magnitudes is

$$1.0857 \times \left( \frac{\sigma_{fc}^2}{f^2 c^2} \right)^{1/2} \text{ mag} \quad (\text{A32})$$

## REFERENCES

- Ajhar, E. A. & Tonry, J. L. 1994, ApJ, 429, 557
- Alongi, M., Bertelli, G., Bressan, A., Chiosi, C., Fagotto, F., Greggio, L., & Nasi, E. 1993, A&AS, 97, 851
- Blakeslee, J. P., Vazdekis, A., & Ajhar, E. A. 2001, MNRAS, 320, 193

- Bressan, A., Fagotto, F., Bertelli, G., & Chiosi, C. 1993, A&AS, 100, 647
- Bruzual A., G. 2002, in Extragalactic Star Clusters, IAU Symposium Ser., Vol. 207, eds. D. Geisler, E. K. Grebel, & D. Minniti (Provo:ASP), 616
- Bruzual, A. G., & Charlot, S. 2003, MNRAS, 344, 1000
- Buzzoni, A. 1989, ApJS, 71, 817
- \_\_\_\_\_ .1993, A&A, 275, 433
- Cantiello, M., Raimondo, G., Brocato, E., & Capaccioli, M. 2003, AJ, 125, 2783
- Cerviño, M., Valls-Gabaud, D., Luridiana, V., & Mas-Hesse, J. M. 2002, A&A, 381, 51
- Cerviño, M. & Valls-Gabaud, D. 2003, MNRAS, 338, 481
- Chabrier, G. 2003, PASP, 115, 763
- Charlot, S. & Fall, S. M. 2000, ApJ, 539, 718
- Charlot, S., Worthey, G., & Bressan, A. 1996, ApJ, 457, 625
- Cohen, J. G. 1982, ApJ, 258, 143
- Cutri, R. M. 2003, Explanatory Supplement to the 2MASS All Sky Data Release,  
<http://www.ipac.caltech.edu/2mass/releases/allsky/doc/expsup.html>
- Elson, R. A. W. & Fall, S. M. 1985, ApJ, 299, 211
- \_\_\_\_\_ .1988, AJ, 96, 1383
- Faber, S. M. & Jackson, R. E. 1976, ApJ, 204, 668
- Fagotto, F., Bressan, A., Bertelli, G., & Chiosi, C. 1994, A&AS, 104, 365
- \_\_\_\_\_ .1994, A&AS, 105, 29
- Ferrarese, L. et al. 2000, ApJS, 128, 431
- Ferraro, F. R., Fusi Pecci, F., Testa, V., Greggio, L., Corsi, C. E., Buonanno, R., Terndrup, D. M., & Zinnecker, H. 1995, MNRAS, 272, 391
- Ferraro, F. R., Montegriffo, P., Origlia, L., & Fusi Pecci, F. 2000, AJ, 119, 1282
- Frogel, J. A., Persson, S. E., & Cohen, J. G. 1980, ApJ, 239, 495
- Girardi, L., Bressan, A., Chiosi, C., Bertelli, G., & Nasi, E. 1996, A&AS, 117, 113
- Graham, A. W., Colless, M. M., Busarello, G., Zaggia, S., & Longo, G. 1998, A&AS, 133, 325

- Harris, W. E. 1996, AJ, 112, 1487
- Iben, I. J. 1967, ARA&A, 5, 571
- Jensen, J. B., Tonry, J. L., Barris, B. J., Thompson, R. I., Liu, M. C., Rieke, M. J., Ajhar, E. A., & Blakeslee, J. P. 2003, ApJ, 583, 712
- Kuchinski, L. E. & Frogel, J. A. 1995, AJ, 110, 2844
- Kuntschner, H. 1998, Ph.D. thesis, University of Durham, UK.
- \_\_\_\_\_. 2000, MNRAS, 315, 184
- Lejeune, T., Cuisinier, F., & Buser, R. 1997, A&AS, 125, 229
- \_\_\_\_\_. 1998, A&AS, 130, 65
- Liu, M. C., Charlot, S., & Graham, J. R. 2000, ApJ, 543, 644
- Liu, M. C. & Graham, J. R. 2001, ApJ, 557, L31
- Liu, M. C., Graham, J. R., & Charlot, S. 2002, ApJ, 564, 216
- Mould, J. R. et al. 2000, ApJ, 529, 786
- Ochsenbein, F., Bauer, P., & Marcout, J. 2000, A&AS, 143, 23
- Persson, S. E., Aaronson, M., Cohen, J. G., Frogel, J. A., & Matthews, K. 1983, ApJ, 266, 105
- Prugniel, P. & Simien, F. 1996, A&A, 309, 749
- Raimondo, G., Brocato, E., Cantiello, M. & Capaccioli, M. 2003, “A New Theoretical Approach to Evaluate Surface Brightness Fluctuations in Stellar Systems,” poster paper in Stellar Populations 2003, conference, Garching, Germany, October 6–10, 2003
- Renzini, A. 2003, personal communication
- Rood, R. T., & Crocker, D. A., “Some Random Unpublished Results of Possible Interest,” <http://www.astro.virginia.edu/~rtr/papers/>
- Santos, J. F. C. & Frogel, J. A. 1997, ApJ, 479, 764
- Schlegel, D. J., Finkbeiner, D. P., & Davis, M. 1998, ApJ, 500, 525
- Searle, L., Wilkinson, A., & Bagnuolo, W. G. 1980, ApJ, 239, 803
- Skrutskie, M. F. et al. 1997, ASSL Vol. 210: The Impact of Large Scale Near-IR Sky Surveys, 25
- Stephens, A. W., Frogel, J. A., Ortolani, S., Davies, R., Jablonka, P., Renzini, A., & Rich, R. M. 2000, AJ, 119, 419

- Stetson, P. B. 1987, PASP, 99, 191
- Sweigart, A. V. & Gross, P. G. 1978, ApJS, 36, 405
- Tonry, J. L., Blakeslee, J. P., Ajhar, E. A., & Dressler, A. 1997, ApJ, 475, 399
- Tonry, J. & Schneider, D. P. 1988, AJ, 96, 807
- van den Bergh, S. 1981, A&AS, 46, 79
- VandenBerg, D. A. & Bell, R. A. 1985, ApJS, 58, 561
- Welch, D. L. 1991, AJ, 101, 538
- Westera, P. 2001, Ph.D. Thesis, University of Basel
- Westera, P., Lejeune, T., Buser, R., Cuisinier, F., & Bruzual, G. 2002, A&A, 381, 524
- Worthey, G. 1993a, ApJ, 409, 530
- \_\_\_\_\_. 1993b, ApJ, 418, 947

Fig. 1.— Comparison between the stellar transformation from *HST* NICMOS Camera 2 *F160W* to CIT/CTIO *H* (Stephens et al. (2000), *dotted lines*), and the SBF transformations derived from stellar population synthesis models. *Top panels*: solar metallicity; *bottom panels*:  $Z = 0.05$ . *Left column*:  $\bar{H} - \overline{F160W}$  vs  $(J - K)$ ; *middle column*: vs  $(J - K)_{bright}$  of stars brighter than  $M_K = -4.5$ ; *right column*: vs  $(\bar{J} - \bar{K})$ . The model transformations are closest to the stellar transformation when using the color of the brightest stars;  $(J - K_s)_{bright}$  is about 0.48 mag redder than the color of the whole population for  $0.85 \geq (J - K_s) \leq 0.95$ .

Fig. 2.— MC superclusters. Greyscale versions of *J*, *H*, and *K<sub>s</sub>* color mosaics built with 2MASS data. N is up and E is to the left; images are 3'3 on the side.

Fig. 3.— Color–magnitude diagrams of MC superclusters. Stars within 60 arcsec from the center (at the distance of the LMC). Average photometric errors are 0.04 mag in brightness and 0.02 mag in color for sources with  $K_s \leq 13$ ; 0.06 and 0.03 mag for stars with  $13 < K_s \leq 14$ ; and 0.13 and 0.07 mag (about the size of the dots) for sources with  $14 < K_s \leq 15$ .

Fig. 4.— Comparison between contributions from all stars in the isochrone and only from stars brighter than  $M_{K_s} = -4.5$  (or  $K_s = 14$  at the LMC). *Top left panel*:  $Z = 0.0004$ ; *top right panel*:  $Z = 0.004$ ; *bottom left panel*:  $Z = 0.008$ ; *bottom right panel*:  $Z = 0.05$ . Within each panel, difference in magnitudes at *J* (*solid line*), *H* (*dotted line*), *K<sub>s</sub>* (*dashed line*),  $\bar{J}$  (*long-dashed line*),  $\bar{H}$  (*dotted-dashed line*), and  $\bar{K}_s$  (*dotted-long-dashed line*).

Fig. 5.— Systematic errors in MC supercluster parameters. *Top*: *H*-band SBF measurements vs log (age) of all eight MC superclusters; *middle*:  $(\bar{H} - \bar{K}_s)$  colors; *bottom*: ratio of observed to model contributions of stars brighter than  $M_{K_s} = -4.5$  to integrated light at *H*. *Left panels*: Point sources with bad photometry have been eliminated. *Right panels*: All point sources from the PSC have been included. Dots of different colors represent values obtained from different radial ranges. Error bars are Poisson. Lines that represent models with different metallicities (see Figures 7 and 9) are included in top and middle panels.

Fig. 6.— *Left*: comparison of integrated colors vs log(age) with stellar population synthesis models. *Top*:  $(J - H)$ ; *middle*:  $(H - K_s)$ ; *bottom*:  $(J - K_s)$ . Filled symbols are MC clusters from this work, and open ones are Fornax Cluster galaxies whose colors we derived from the 2MASS Extended Source Catalog. Models of a fixed metallicity have the same symbol, with increasing symbol size representing increasing age. Models have  $Z = 0.0004, 0.004, 0.008$ , and  $0.05$ ; they are 1, 10, 50 and 500 Myr, 2, 5, 8, and 17 Gyr old. *Right*: the same data points are plotted with error bars. The values in parentheses are the number of objects in each group.

Fig. 7.— *Left*: comparison of *J*-band (*top*), *H*-band (*middle*), and *K<sub>s</sub>*-band (*bottom*) SBF measurements vs age with stellar population synthesis models. Models and symbols are the same as in Figure 6. *Right*: the same data points are plotted with error bars. The values in parentheses are the number of objects in each group with SBF measurements.

Fig. 8.—  $K_s$  magnitudes in an arbitrary scale, vs main sequence turn-off mass and log (age), for a population with  $Z = 0.0004$ . *Solid line*: average of the RGB; *short-dashed line*: TRGB; *dotted line*: mode of the RGB luminosity function.

Fig. 9.— *Top*: Comparison of SBF colors vs log (age) with stellar population synthesis models. Models and symbols are the same as in previous figures. *Left*:  $(\bar{J} - \bar{H})$ ; *middle*:  $(\bar{H} - \bar{K}_s)$ ; *right*:  $(\bar{J} - \bar{K}_s)$ . *Bottom*: the same data points are plotted with error bars. The values in parentheses are the number of objects in each group with SBF measurements. Dashed lines are best fits to MC star clusters; dotted line is best fit of  $(\bar{H} - \bar{K}_s)$  vs log (age) for MC superclusters and Fornax galaxies (see text).

Fig. 10.— Evolution of the RGB plus AGB average  $K_s$  magnitude (arbitrary scale) vs average color, between 400 Myr (top of lines) and 20 Gyr (bottom of lines), for populations with different metallicities. *Solid line*:  $Z = 0.004$ ; *dotted line*:  $Z = 0.008$ ; *short-dashed line*:  $Z = 0.05$ . Tick marks at 0.4, 1, 4, 16, and 20 Gyr.

Fig. 11.— *Left*: comparison of  $J$ -band (*top*),  $H$ -band (*middle*), and  $K_s$ -band (*bottom*) SBF measurements vs metallicity with stellar population synthesis models. Models and symbols are the same as in previous figures. Lines connect models with the same age; models are 50 and 500 Myr, 2, 5, 8, and 17 Gyr old. *Middle*: the same data points are plotted with error bars. The values in parentheses are the number of objects in each group with SBF measurements. *Right*: the scale has been changed to show loci of 1 and 10 Myr old models; insets show location of plots in the left and middle.

Fig. 12.— *Top left*: comparison of  $(\bar{H} - \bar{K}_s)$  SBF color vs metallicity of MC superclusters with stellar population synthesis models. Models, symbols, and lines are the same as in figure 11. *Bottom left*: comparison of  $(\bar{H} - \bar{K}_s)$  SBF color vs metallicity of MC superclusters and Fornax Cluster galaxies with stellar population synthesis models; the scale has been changed relative to the top left panel to allow for the inclusion of the galaxies. Models and symbols are the same as in previous figures. The green error bars represent the galaxy average, which is only marginally consistent with the models between 5 and 17 Gyr old. *Middle*: the same data points are plotted with error bars. The values in parentheses are the number of objects. *Right*: the scale has been changed anew to show loci of 1 and 10 Myr old models; insets show location of plots in the left and middle.

Table 1. Cluster Data

Supercluster	Age (yr)	Z	Region	Name	$N_*$	s-parameter	Cloud	$E(B - V)$	SWB-class
Pre-SWB ...	$2.4 \times 10^6$	0.01	$0'' - 60''$	IC 2128	9	1	LMC	0.15	
				NGC 1748	16	1	LMC		
				NGC 1743	19	2	LMC		
				L 107	3	3	SMC		
				NGC 1714	6	3	LMC		
				NGC 1727 <sup>a</sup>	22	4	LMC		
				NGC 1910 <sup>a</sup>	34	4	LMC		
				NGC 1936 (IC 2127) <sup>a</sup>	8	4	LMC		
				L 84 <sup>a</sup>	25	5	SMC		
				NGC 602	6	6	SMC		
				NGC 2001 <sup>a</sup>	20	6	LMC		
				NGC 1833 <sup>a</sup>	17	7	LMC		
				NGC 2027	12	7	LMC		
				SL 362 <sup>a</sup>	39	7	LMC		
				NGC 2014 <sup>b</sup>	10	8	LMC		
				NGC 346	15	8	SMC		
				HS 314	31	10	LMC		
				NGC 2074 <sup>b</sup>	20	10	LMC		
				SL 360 <sup>a</sup>	33	10	LMC		
				NGC 1984	25	11	LMC		
				NGC 2018	20	11	LMC		
				NGC 1873 <sup>a</sup>	10	12	LMC		
				L 70	8	13	SMC		
				NGC 2006	9	13	LMC		

Table 1—Continued

Supercluster	Age (yr)	Z	Region	Name	$N_*$	s-parameter	Cloud	$E(B - V)$	SWB-class
SWB I.....	$1 \times 10^7$	0.01	$0'' - 60''$	NGC 1983	28	13	LMC		
				NGC 2011	4	13	LMC	0.08	
				SL 114	24	13	LMC		
				L 74	10	14	SMC		
				NGC 2003	2	15	LMC		
				L 51	7	15	SMC		
				L 48	3	15	SMC		
				NGC 1994	22	15	LMC	0.14	
				NGC 2004	15	15	LMC	0.06	I
				SL 538	10	15	LMC		
				L 56	15	16	SMC		II
				NGC 290	20	16	SMC		
				NGC 1767	25	16	LMC	0.15	
				NGC 1787	20	16	LMC		
				NGC 2009	13	16	LMC		
				NGC 2098	9	16	LMC		
				L 45 <sup>a</sup>	15	17	SMC		
				NGC 1766	11	17	LMC		
				NGC 1772	24	17	LMC		
				NGC 1805	12	17	LMC	0.10	
				NGC 2002	5	17	LMC		
				NGC 2100	21	17	LMC	0.24	I
				L 66	15	18	SMC		
				NGC 1810	12	18	LMC		

Table 1—Continued

Supercluster	Age (yr)	Z	Region	Name	$N_*$	s-parameter	Cloud	$E(B - V)$	SWB-class
SWB II....	$5 \times 10^7$	0.01	0''— 60''	NGC 1818	11	18	LMC	0.10	I
				NGC 330	22	19	SMC		I
				NGC 176	8	20	SMC		
				NGC 299	9	20	SMC		I
				NGC 1704	10	20	LMC		
				NGC 1711	9	20	LMC	0.16	II
				NGC 1860	40	20	LMC		
				NGC 376	21	20	SMC		
				SL 477	12	20	LMC		
				NGC 1869	12	21	LMC		
				NGC 1698	15	21	LMC		
				NGC 1847	32	21	LMC		
				NGC 1850	43	21	LMC	0.15	
				NGC 1863	37	21	LMC		
				SL 106	25	21	LMC		
				IC 1612	16	22	SMC		
				L 39	18	22	SMC		
				NGC 220	9	22	SMC		III
				NGC 222	8	22	SMC		II-III
				NGC 1735	14	22	LMC		
				NGC 1793	16	22	LMC		
				NGC 1834	42	22	LMC		
				NGC 1855	65	22	LMC	0.12	
				NGC 1928 <sup>a</sup>	46	22	LMC		

Table 1—Continued

Supercluster	Age (yr)	Z	Region	Name	$N_*$	s-parameter	Cloud	$E(B - V)$	SWB-class
				NGC 2214 <sup>a</sup>	14	22	LMC	0.10	II
				IC 1624	21	23	SMC		
				NGC 1774	15	23	LMC	0.10	II
				NGC 1782	21	23	LMC		
				NGC 1804	29	23	LMC		
				NGC 1903 <sup>a</sup>	34	23	LMC		
				NGC 2164	25	23	LMC	0.10	III
				IC 1655 <sup>c</sup>	5	24	SMC		
				NGC 231	12	24	SMC		
				NGC 242	13	24	SMC		II
				NGC 422	6	24	SMC		
				NGC 1732	12	24	LMC		
				NGC 1755	16	24	LMC	0.12	II-III
				NGC 1854	64	24	LMC	0.13	II
				NGC 1870	30	24	LMC		
				NGC 1913 <sup>a</sup>	30	24	LMC		
				NGC 1951	17	24	LMC	0.10	
				NGC 1986	52	24	LMC	0.18	II
				NGC 2118	12	24	LMC		
				SL 56	10	24	LMC		
SWB III....	$5 \times 10^8$	0.01	0''— 60''	IC 1660	5	25	SMC		
				L 44	30	25	SMC		
				L 63	16	25	SMC		
				NGC 256	14	25	SMC		II

Table 1—Continued

Supercluster	Age (yr)	Z	Region	Name	$N_*$	s-parameter	Cloud	$E(B - V)$	SWB-class
				NGC 458	23	25	SMC		III
				NGC 1828	34	25	LMC		
				NGC 1844	20	25	LMC		
				NGC 1943 <sup>a</sup>	41	25	LMC	0.18	
				NGC 2000	20	25	LMC		
				NGC 2041	15	25	LMC	0.05	III
				NGC 2157	17	25	LMC	0.10	
				NGC 2159	17	25	LMC	0.10	
				NGC 2172	10	25	LMC	0.10	
				SL 539	27	25	LMC		
				IC 1611 <sup>a</sup>	17	26	SMC		
				NGC 265	33	26	SMC		III
				NGC 2058	57	26	LMC	0.18	III
				NGC 2065	65	26	LMC	0.18	III
				NGC 2136	31	26	LMC	0.10	III
				NGC 2156	11	26	LMC	0.10	
				L 40 <sup>a</sup>	20	27	SMC		
				NGC 1866	37	27	LMC	0.10	III
				NGC 2025	26	27	LMC		
				NGC 2031	38	27	LMC		
				L 114	4	28	SMC		
				NGC 1775 <sup>a</sup>	18	28	LMC		
				NGC 1885	46	28	LMC		
				NGC 1895 <sup>a</sup>	10	28	LMC		

Table 1—Continued

Supercluster	Age (yr)	Z	Region	Name	$N_*$	s-parameter	Cloud	$E(B - V)$	SWB-class
SWB IV ....	$1 \times 10^9$	0.01	$0'' - 60''$	NGC 2134	42	28	LMC	0.10	IV
				NGC 269	15	29	SMC		III-IV
				NGC 1830	35	29	LMC		
				NGC 1953	25	29	LMC	0.12	
				L 53	16	30	SMC		
				NGC 294 (L 47)	24	30	SMC		
				NGC 1801	52	30	LMC		
				NGC 1856 <sup>a</sup>	58	30	LMC	0.24	IV
				NGC 1872	51	30	LMC	0.13	III-IV
				NGC 1831 <sup>a</sup>	6	31	LMC	0.10	V
				NGC 2056	41	31	LMC		
				L 26 <sup>a</sup>	4	32	SMC		
				NGC 1756	29	32	LMC		
				NGC 1849	19	32	LMC		
				NGC 2107	46	32	LMC	0.19	IV
				SL 562	23	32	LMC		
				NGC 1868	5	33	LMC	0.07	
				NGC 2249	11	34	LMC		
				NGC 1987	27	35	LMC	0.12	IV
				NGC 2209	10	35	LMC	0.07	III-IV
				NGC 2108	16	36	LMC	0.18	
				SL 663 <sup>a,b</sup>	15	36	LMC		
SWB V ....	$3 \times 10^9$	0.008	$0'' - 60''$	IC 2146	19	37	LMC		

Table 1—Continued

Supercluster	Age (yr)	Z	Region	Name	$N_*$	s-parameter	Cloud	$E(B - V)$	SWB-class
				NGC 152	21	37	SMC		IV
				NGC 411	15	37	SMC		V-VI
				NGC 1644 <sup>a</sup>	10	37	LMC		
				NGC 1783	33	37	LMC	0.10	V
				NGC 2231	22	37	LMC	0.10	V
				SL 363 <sup>a</sup>	41	37	LMC		
				NGC 419	25	38	SMC		V
				NGC 1777 <sup>b</sup>	10	38	LMC		
				SL 556 <sup>a,b</sup>	18	38	LMC		
				NGC 1651 <sup>a</sup>	20	39	LMC		
				NGC 1917 <sup>a</sup>	36	39	LMC		
				NGC 2154	29	39	LMC	0.10	V
				NGC 2162	8	39	LMC	0.07	V
				NGC 2213	16	39	LMC	0.10	V-VI
				NGC 1806	50	40	LMC	0.12	V
				NGC 1846 <sup>a</sup>	38	40	LMC	0.10	V
				NGC 2193 <sup>b</sup>	16	40	LMC		
				SL 855 <sup>a,b</sup>	8	40	LMC		
				NGC 1795	29	41	LMC		
SWB VI....	$6 \times 10^9$	0.004	0''— 60''	NGC 1751	44	42	LMC	0.12	
				NGC 2173	31	42	LMC	0.07	V-VI
				NGC 1652 <sup>a</sup>	15	43	LMC		
				ESO121-SCO3 <sup>b</sup>	9	44	LMC		
				NGC 2121	47	44	LMC	0.10	VI

Table 1—Continued

Supercluster	Age (yr)	Z	Region	Name	$N_*$	s-parameter	Cloud	$E(B - V)$	SWB-class
				NGC 1718	33	45	LMC		
				NGC 1978	28	45	LMC	0.10	VI
				NGC 1852	33	45	LMC		
				NGC 2155	18	45	LMC	0.10	VI
				SL 842 <sup>b</sup>	5	45	LMC		
				L 1 <sup>a</sup>	26	46	SMC		
				NGC 416	25	46	SMC		VI
				NGC 1754	25	46	LMC		
				NGC 1916 <sup>a</sup>	16	46	LMC		
				NGC 2005	43	46	LMC		
				NGC 2019	46	46	LMC	0.18	VII
				SL 506	8	46	LMC		
SWB VII ...	$1.2 \times 10^{10}$	0.0006	0''— 60''	L 11	6	47	SMC		
				L 68	19	47	SMC		
				NGC 121	28	47	SMC		VII
				NGC 1835	48	47	LMC	0.12	VII
				L 8	24	48	SMC		
				NGC 361	17	48	SMC		
				NGC 1786	35	48	LMC	0.12	
				NGC 2210	31	48	LMC	0.10	VII
				L 113	15	49	SMC		
				NGC 339	22	49	SMC		VII
				NGC 1898 <sup>a</sup>	20	50	LMC	0.09	
				H 11 (SL 868)	20	51	LMC	0.10	VII

Table 1—Continued

Supercluster	Age (yr)	Z	Region	Name	$N_*$	s-parameter	Cloud	$E(B - V)$	SWB-class

Note. — Col. (2) and (3). Ages and metallicities of superclusters from Cohen (1982); for the Pre-SWB supercluster only, we have adopted the age of a cluster with  $s = 7$  from Elson & Fall (1985). Col. (5). Number of stars from the 2MASS PSC included in analysis. Col. (7).  $s$ -parameter from Elson & Fall (1985, 1988). Col. (9).  $E(B - V)$  from Persson et al. (1983); otherwise, we have assumed  $E(B - V) = 0.075$ , and  $E(B - V) = 0.037$  for the SMC (Schlegel et al. 1998). Col. (10). SWB class from Searle, Wilkinson, & Bagnuolo (1980).

<sup>a</sup> Data from All Sky Data Release of 2MASS.

<sup>b</sup> Clusters added to sample from Elson & Fall (1988).

<sup>c</sup> Listed as IC 1665 in both van den Bergh (1981), and Elson & Fall (1985).

Table 2. Fornax Cluster Galaxies

Name	$\bar{M}_{K_s}^{I-SBF}$	$\bar{M}_{F160W}^{I-SBF}$	$\bar{M}_H$	$J$	$H$	$K_s$	Age (Gyr)	[Fe/H]
IC 2006	-5.83 ± 0.31	-4.82 ± 0.29	-5.09 ± 0.31	9.575± 0.019	8.866± 0.018	8.638± 0.013	6.0±2.1	0.25±0.15
NGC 1336	-5.67 ± 0.31	...	...	10.948± 0.022	10.255± 0.020	10.031± 0.028	9.0±3.1	-0.12±0.15
NGC 1339	-5.76 ± 0.36	-5.02 ± 0.36	-5.28 ± 0.37	9.665± 0.018	8.998± 0.012	8.771± 0.014	8.0±2.8	0.15±0.15
NGC 1351	-5.68 ± 0.19	-4.77 ± 0.17	-5.02 ± 0.20	9.610± 0.018	8.931± 0.013	8.745± 0.015	10.5±3.6	0.00±0.15
NGC 1373	-6.67 ± 0.60	-5.2 ± 0.5	-5.5 ± 0.5	11.538± 0.021	10.878± 0.021	10.693± 0.028	9.5±3.3	0.00±0.15
NGC 1374	-5.82 ± 0.14	-4.82 ± 0.18	-5.08 ± 0.21	9.134± 0.017	8.446± 0.012	8.242± 0.012	11.0±3.8	0.05±0.15
NGC 1375	-6.06 ± 0.29	-5.47 ± 0.15	-5.72 ± 0.18	10.635± 0.019	10.000± 0.017	9.766± 0.021	1.5±0.5	0.30±0.15
NGC 1379	-5.85 ± 0.17	-5.11 ± 0.19	-5.36 ± 0.21	9.263± 0.018	8.606± 0.012	8.396± 0.013	8.0±2.8	-0.02±0.15
NGC 1380	-5.84 ± 0.18	-4.64 ± 0.19	-4.91 ± 0.22	8.042± 0.017	7.355± 0.011	7.092± 0.010	6.3±2.2	0.28±0.15
NGC 1404	-5.72 ± 0.20	-4.76 ± 0.21	-5.03 ± 0.23	7.838± 0.017	7.149± 0.011	6.902± 0.010	5.0±1.7	0.30±0.15
NGC 1427	-6.40 ± 0.25	-5.28 ± 0.25	-5.53 ± 0.27	9.089± 0.019	8.399± 0.018	8.223± 0.012	7.0±2.4	0.15±0.15

 38  
|

Note. — Col. (2). Absolute  $K_s$  fluctuation magnitude from Liu, Graham, & Charlot (2002). Col. (3). Absolute  $F160W$  fluctuation magnitude from Jensen et al. (2003). Col. (3). Absolute  $H$  fluctuation magnitude calculated from  $F160W$  values via the transformations in Stephens et al. (2000) (see text). Col. (5), (6), and (7).  $J$ ,  $H$ , and  $K_s$  magnitudes from 2MASS Extended Source Catalog (XSC). Col. (8) and (9). Ages and abundances from Kuntschner (1998); errors of ±0.15 dex in ages and abundances are averages taken from Figure 12 in Kuntschner (2000).

Table 3. Results I: Supercluster integrated magnitudes and colors

Supercluster	$N_{\text{cl}}$	Age (yr)	Z	Mass ( $10^6 M_{\odot}$ )	$M_J$	$M_H$	$M_{K_s}$	$(J - H)$	$(J - K_s)$	$(H - K_s)$
Pre-SWB ..	28	$2.4 \pm 1.7 \times 10^6$	$0.010 \pm 0.005$	$1.1 \pm 0.4$	$-12.79 \pm 0.09$	$-13.23 \pm 0.10$	$-13.58 \pm 0.09$	$0.47 \pm 0.04$	$0.81 \pm 0.04$	$0.34 \pm 0.03$
SWB I .....	29	$1.0 \pm 0.7 \times 10^7$	$0.010 \pm 0.005$	$0.53 \pm 0.06$	$-13.59 \pm 0.07$	$-14.22 \pm 0.07$	$-14.45 \pm 0.07$	$0.63 \pm 0.03$	$0.86 \pm 0.03$	$0.23 \pm 0.03$
SWB II .....	35	$5 \pm 3 \times 10^7$	$0.010 \pm 0.005$	$0.96 \pm 0.09$	$-13.12 \pm 0.07$	$-13.69 \pm 0.07$	$-13.85 \pm 0.08$	$0.57 \pm 0.03$	$0.72 \pm 0.04$	$0.15 \pm 0.03$
SWB III .....	32	$5 \pm 3 \times 10^8$	$0.010 \pm 0.005$	$2.0 \pm 0.1$	$-12.67 \pm 0.06$	$-13.18 \pm 0.08$	$-13.37 \pm 0.08$	$0.51 \pm 0.04$	$0.70 \pm 0.04$	$0.18 \pm 0.03$
SWB IV .....	18	$1.0 \pm 0.7 \times 10^9$	$0.010 \pm 0.005$	$2.0 \pm 0.2$	$-11.90 \pm 0.07$	$-12.53 \pm 0.09$	$-12.73 \pm 0.09$	$0.64 \pm 0.04$	$0.83 \pm 0.05$	$0.19 \pm 0.04$
SWB V .....	20	$3 \pm 2 \times 10^9$	$0.008 \pm 0.004$	$4.2 \pm 0.2$	$-12.41 \pm 0.05$	$-13.07 \pm 0.05$	$-13.33 \pm 0.06$	$0.66 \pm 0.03$	$0.92 \pm 0.04$	$0.26 \pm 0.03$
SWB VI .....	17	$6 \pm 4 \times 10^9$	$0.004 \pm 0.002$	$5.8 \pm 0.1$	$-12.37 \pm 0.05$	$-12.97 \pm 0.05$	$-13.14 \pm 0.06$	$0.61 \pm 0.03$	$0.78 \pm 0.04$	$0.17 \pm 0.03$
SWB VII ..	12	$1.2 \pm 0.8 \times 10^{10}$	$0.0006 \pm 0.0003$	$7.6 \pm 0.1$	$-12.14 \pm 0.05$	$-12.66 \pm 0.05$	$-12.74 \pm 0.05$	$0.52 \pm 0.03$	$0.60 \pm 0.03$	$0.08 \pm 0.03$

Note. — Col. (2). Number of clusters in each supercluster. Col. (3) and (4). Ages and metallicities of superclusters, and their errors, from Cohen (1982). Col. (5) Masses from theoretical near-IR mass-to-light ratios; errors are equal to the dispersion of the results at  $J$ ,  $H$ , and  $K_s$ .

Table 4. Results II: Supercluster fluctuation magnitudes and colors

Supercluster	$N_{\text{cl}}$	Age (yr)	Z	Mass ( $10^6 M_{\odot}$ )	$\bar{M}_J$	$\bar{M}_H$	$\bar{M}_{K_s}$	$(\bar{J} - \bar{H})$	$(\bar{J} - \bar{K}_s)$	$(\bar{H} - \bar{K}_s)$
Pre-SWB ..	28	$2.4 \pm 1.7 \times 10^6$	$0.010 \pm 0.005$	$1.1 \pm 0.4$	$-6.49 \pm 0.42$	$-7.63 \pm 0.43$	$-7.70 \pm 0.40$	$1.14 \pm 0.07$	$1.22 \pm 0.09$	$0.07 \pm 0.05$
SWB I .....	29	$1.0 \pm 0.7 \times 10^7$	$0.010 \pm 0.005$	$0.53 \pm 0.06$	$-7.54 \pm 0.14$	$-8.49 \pm 0.12$	$-8.67 \pm 0.12$	$0.95 \pm 0.06$	$1.13 \pm 0.06$	$0.18 \pm 0.01$
SWB II .....	35	$5 \pm 3 \times 10^7$	$0.010 \pm 0.005$	$0.96 \pm 0.09$	$-6.74 \pm 0.40$	$-7.57 \pm 0.32$	$-7.88 \pm 0.28$	$0.84 \pm 0.10$	$1.14 \pm 0.14$	$0.30 \pm 0.05$
SWB III ....	32	$5 \pm 3 \times 10^8$	$0.010 \pm 0.005$	$2.0 \pm 0.1$	$-6.05 \pm 0.23$	$-7.10 \pm 0.23$	$-7.45 \pm 0.24$	$1.05 \pm 0.04$	$1.39 \pm 0.05$	$0.35 \pm 0.02$
SWB IV ....	18	$1.0 \pm 0.7 \times 10^9$	$0.010 \pm 0.005$	$2.0 \pm 0.2$	$-5.67 \pm 0.22$	$-6.85 \pm 0.21$	$-7.51 \pm 0.18$	$1.18 \pm 0.05$	$1.84 \pm 0.12$	$0.66 \pm 0.09$
SWB V ....	20	$3 \pm 2 \times 10^9$	$0.008 \pm 0.004$	$4.2 \pm 0.2$	$-4.60 \pm 0.14$	$-5.94 \pm 0.16$	$-6.69 \pm 0.20$	$1.34 \pm 0.05$	$2.09 \pm 0.10$	$0.76 \pm 0.06$
SWB VI ....	17	$6 \pm 4 \times 10^9$	$0.004 \pm 0.002$	$5.8 \pm 0.1$	$-4.23 \pm 0.17$	$-5.49 \pm 0.19$	$-6.21 \pm 0.24$	$1.26 \pm 0.07$	$1.98 \pm 0.16$	$0.72 \pm 0.10$
SWB VII ..	12	$1.2 \pm 0.8 \times 10^{10}$	$0.0006 \pm 0.0003$	$7.6 \pm 0.1$	$-3.14 \pm 0.19$	$-4.29 \pm 0.27$	$-4.92 \pm 0.38$	$1.15 \pm 0.10$	$1.78 \pm 0.22$	$0.63 \pm 0.14$

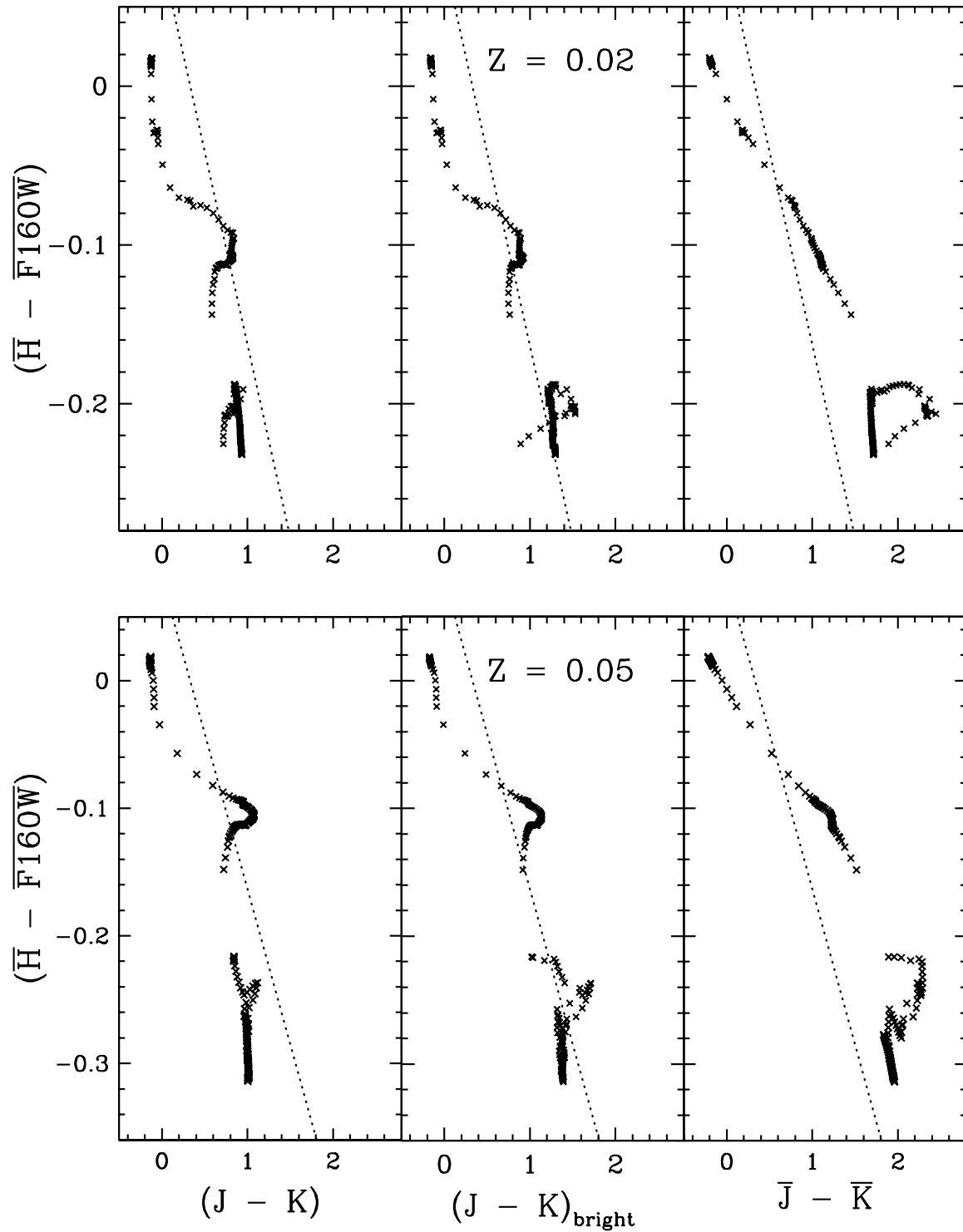
Table 5. Fractional contribution of bright stars to integrated light

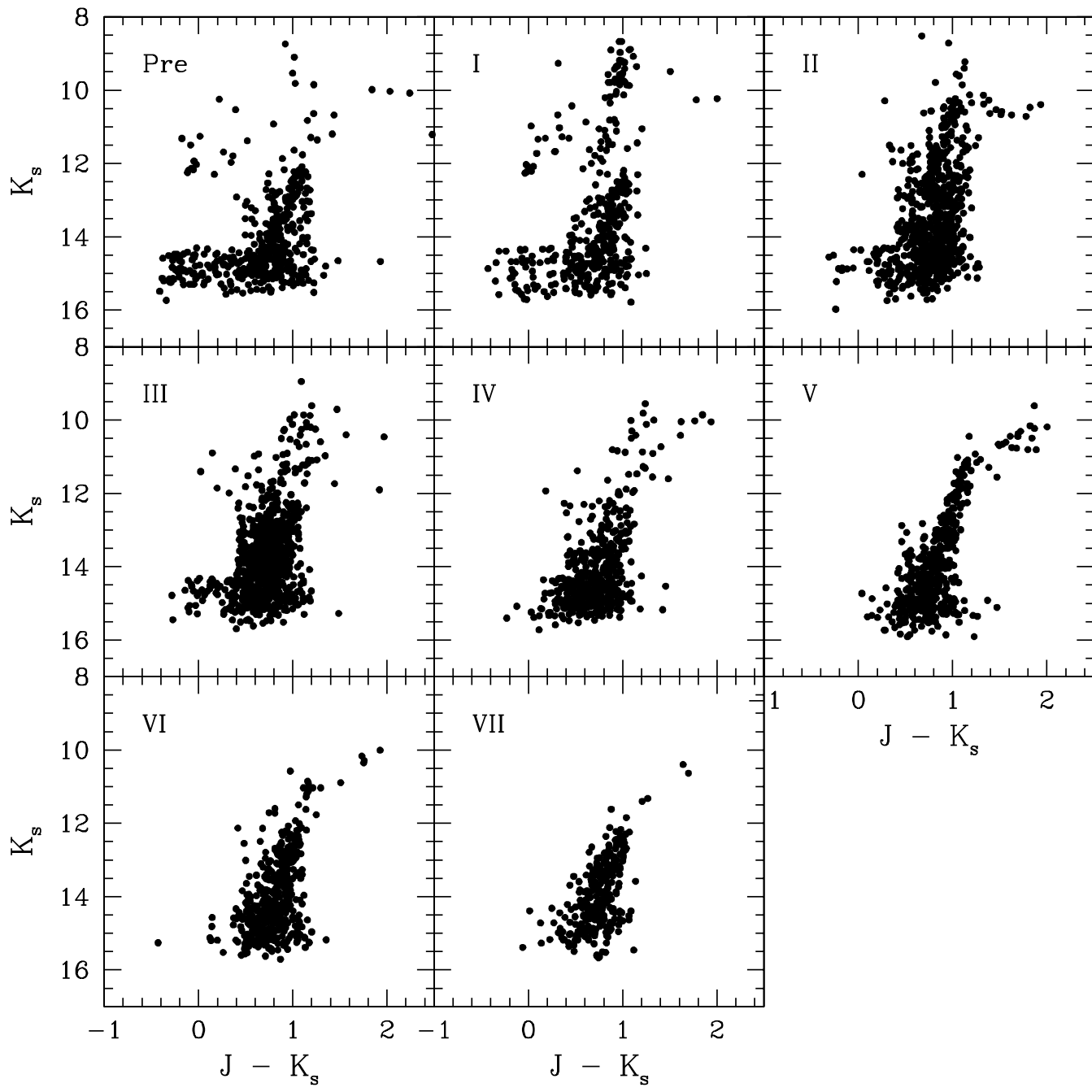
Supercluster	<i>J</i>		<i>H</i>		<i>K<sub>s</sub></i>	
	data	model	data	model	data	model
Pre-SWB ..	47±6%	39±5%	67±9%	39±5%	57±8%	38±6%
SWB I .....	68±6%	85±7%	81±7%	91±7%	78±6%	92±8%
SWB II .....	61±4%	80±5%	71±4%	87±5%	77±4%	88±5%
SWB III ...	63±5%	23±2%	75±6%	36±3%	76±6%	43±3%
SWB IV ...	55±6%	23±2%	64±7%	36±4%	73±8%	43±5%
SWB V .....	36±3%	29±2%	45±4%	39±3%	49±5%	44±4%
SWB VI ...	33±3%	27±2%	40±3%	35±3%	45±4%	39±4%
SWB VII ..	20±2%	20±2%	25±2%	25±2%	27±3%	27±3%

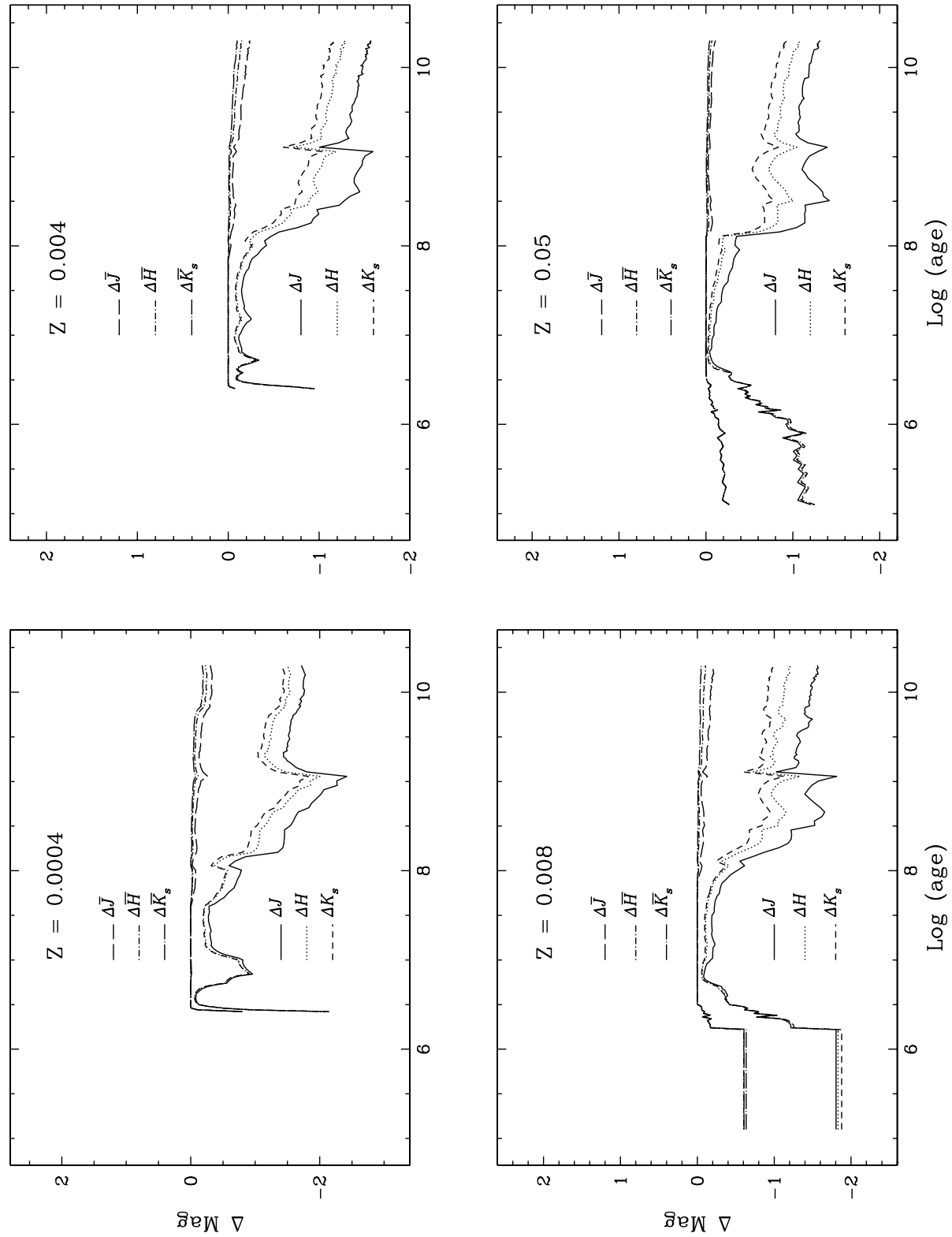
Table 6. Fluctuation color vs log (age/yr)

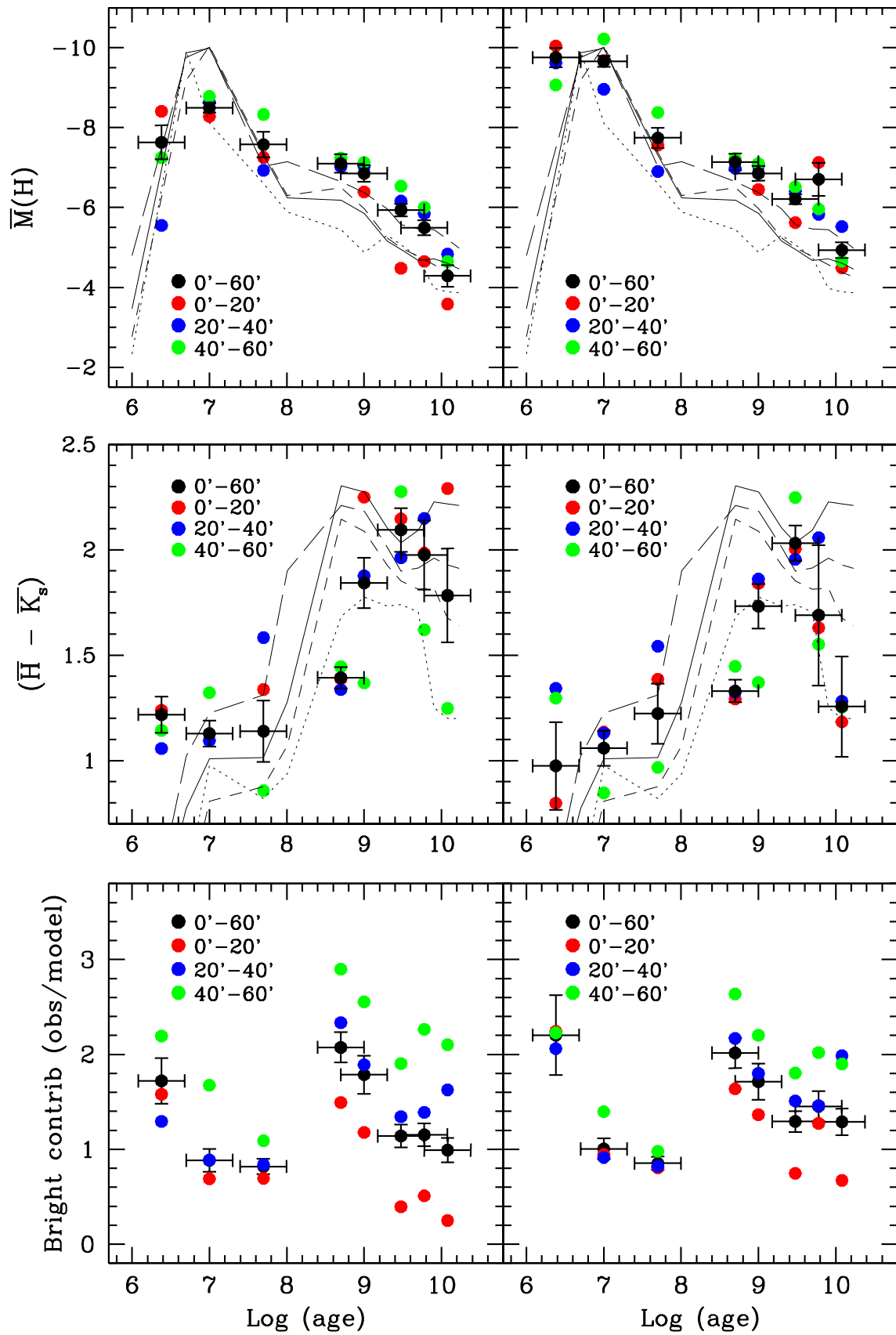
<i>Color</i>	<i>a</i>	<i>b</i>	<i>N</i>	rms	$\tilde{\chi}^2$
$(\overline{J} - \overline{H})$	$0.29 \pm 0.18$	$0.10 \pm 0.02$	8	0.37	2.9
$(\overline{H} - \overline{K_s})$	$-1.29 \pm 0.22$	$0.21 \pm 0.03$	8	0.26	1.2
$(\overline{H} - \overline{K_s})$	$-1.25 \pm 0.16$	$0.20 \pm 0.02$	18	0.76	1.8
$(\overline{J} - \overline{K_s})$	$-0.97 \pm 0.36$	$0.30 \pm 0.04$	8	0.56	2.1

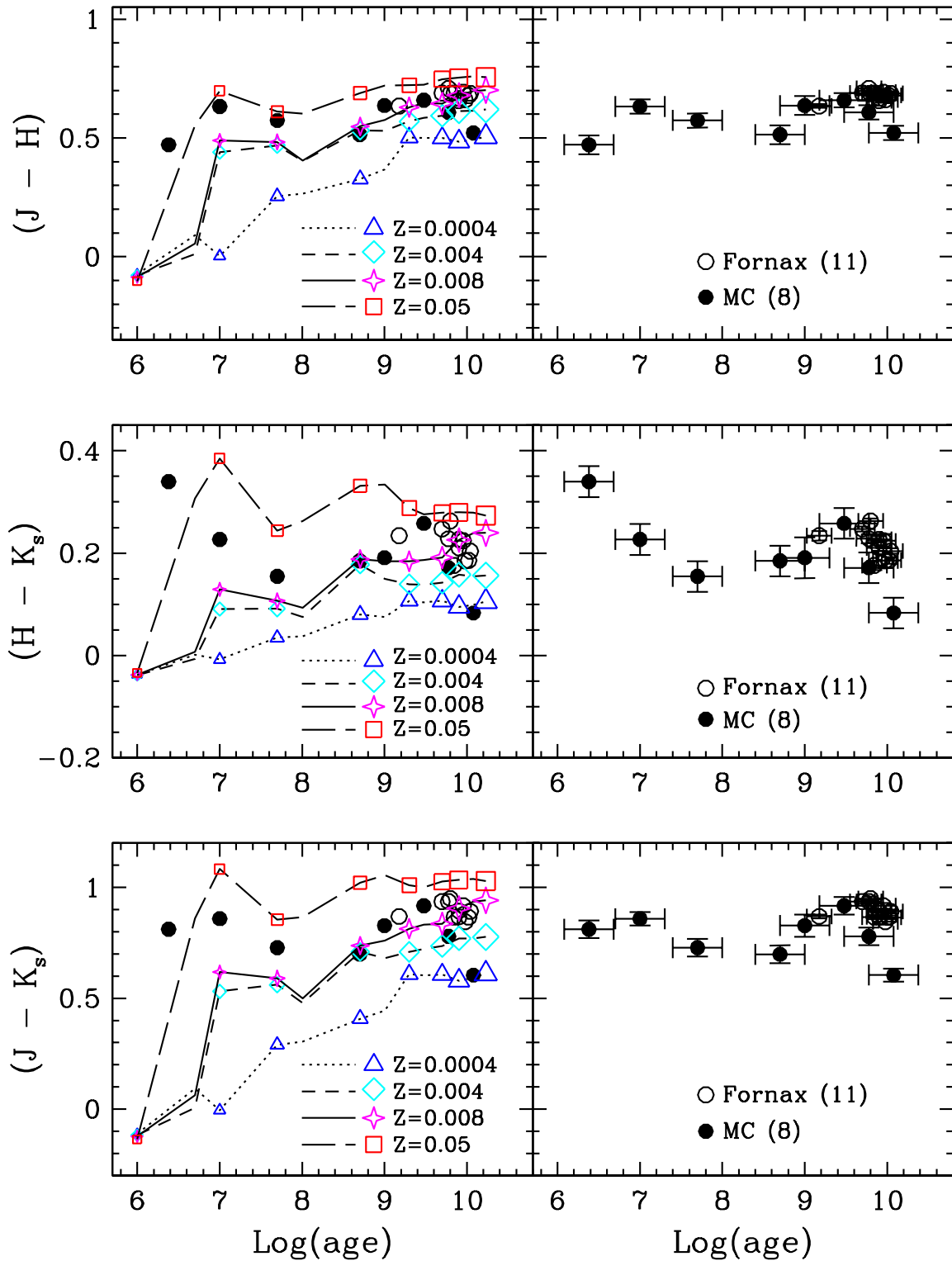
Note. — Fits of fluctuation color vs age of the form  
 $\overline{\text{Color}} = a + b [ \log(\text{age/yr}) ]$ ; the number of objects used for the fit is tabulated as *N*. The resulting rms of the points (in magnitudes) after the fit and the reduced chi-square ( $\tilde{\chi}^2$ ) are also listed.

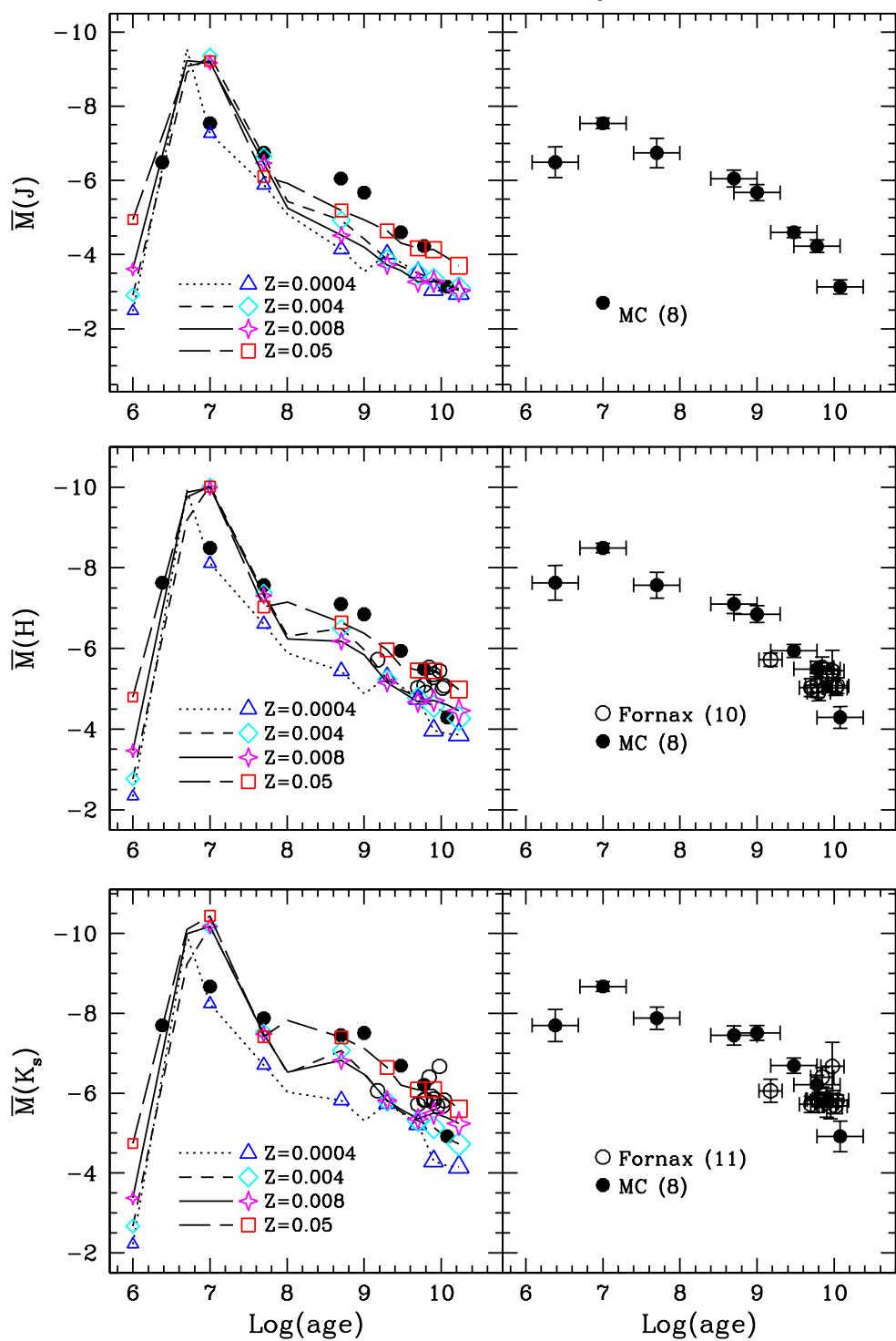


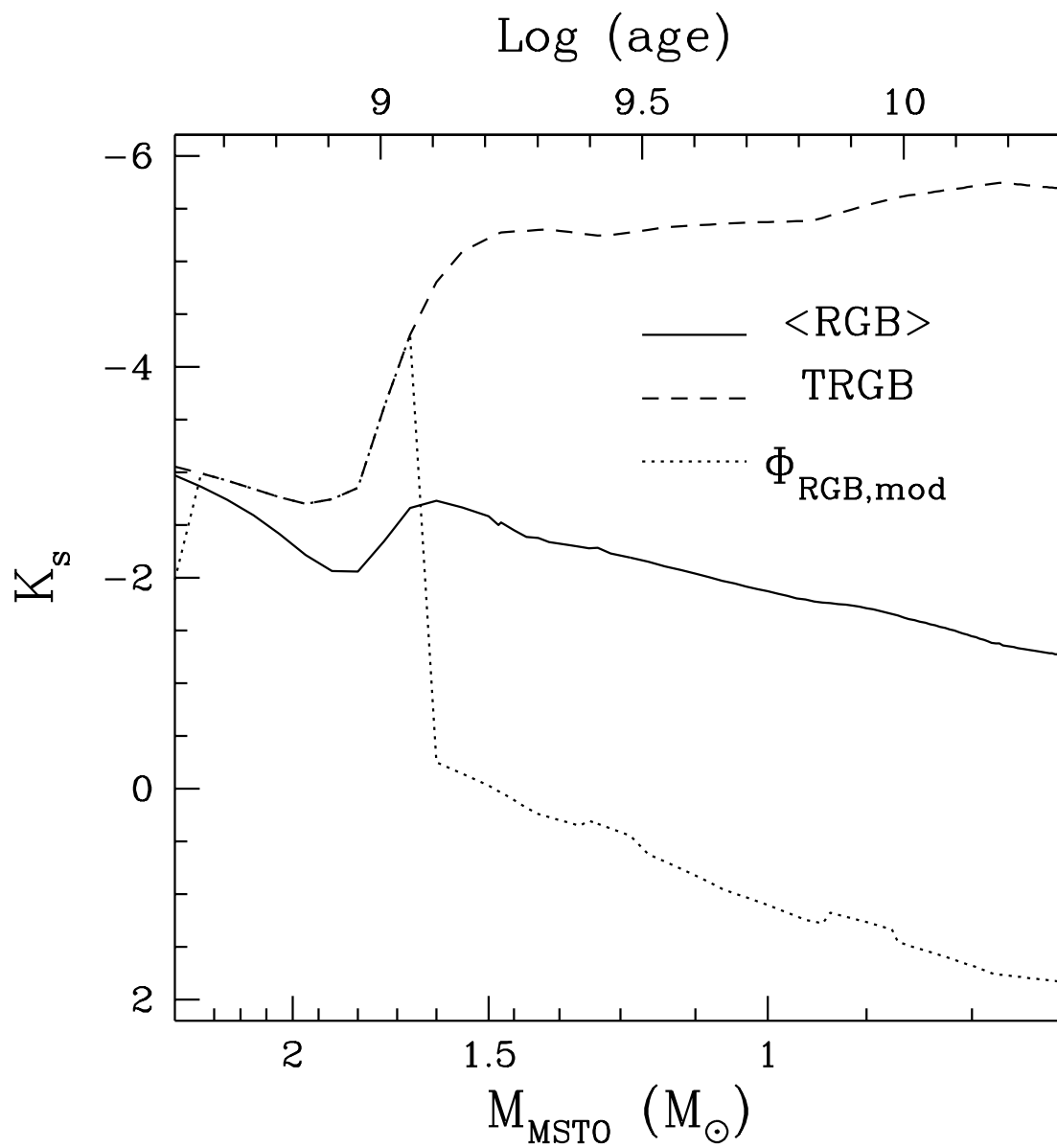


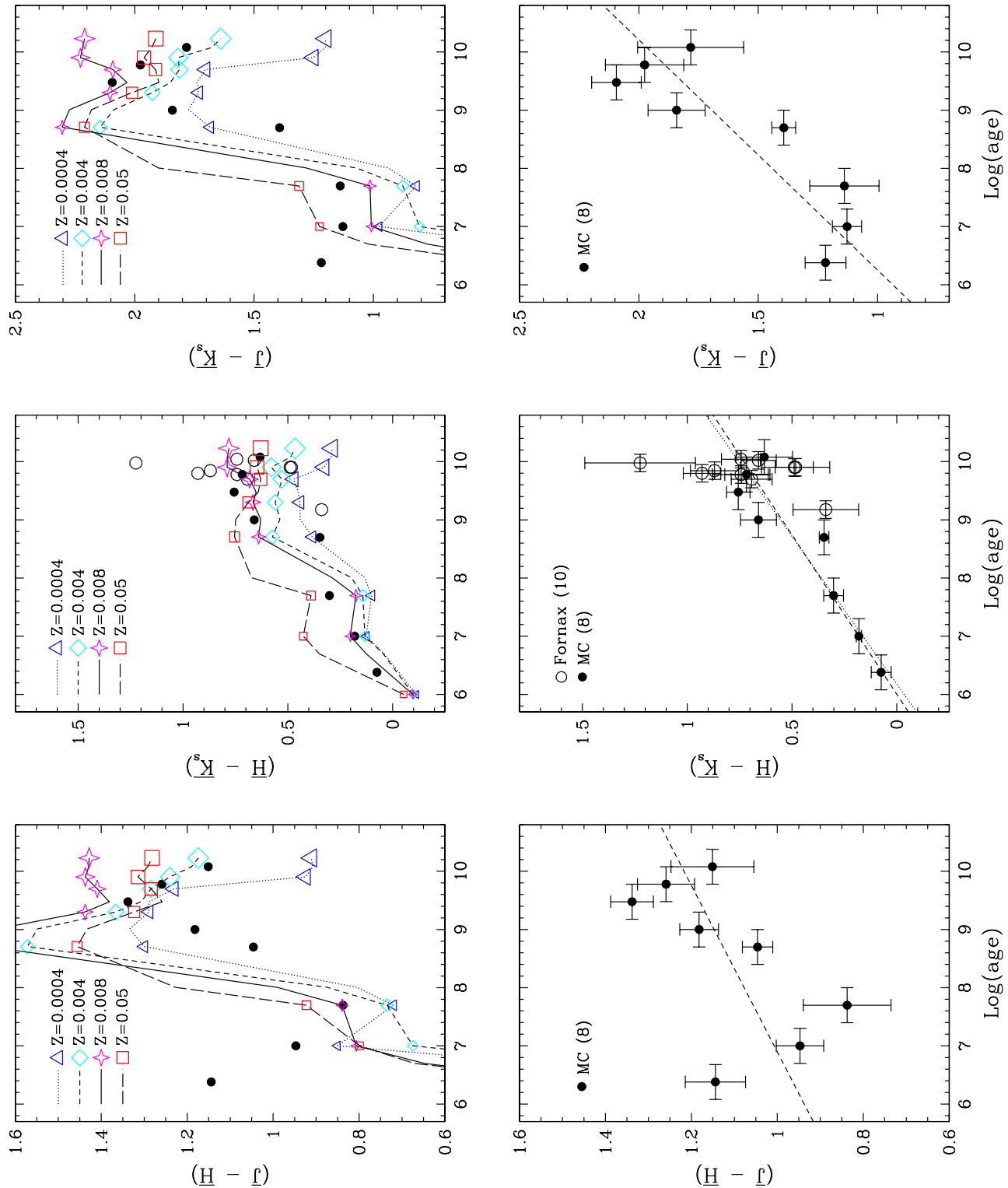


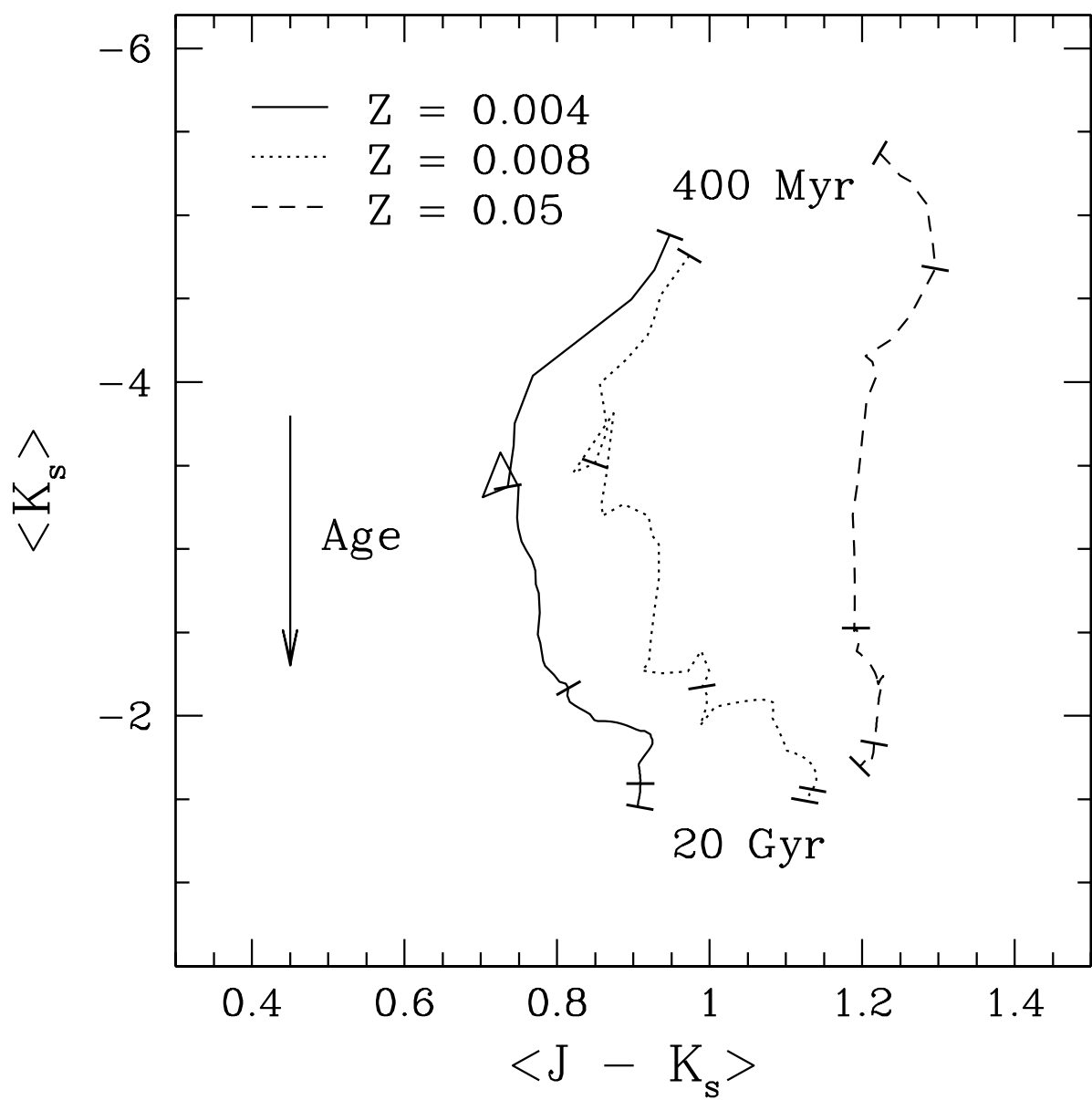


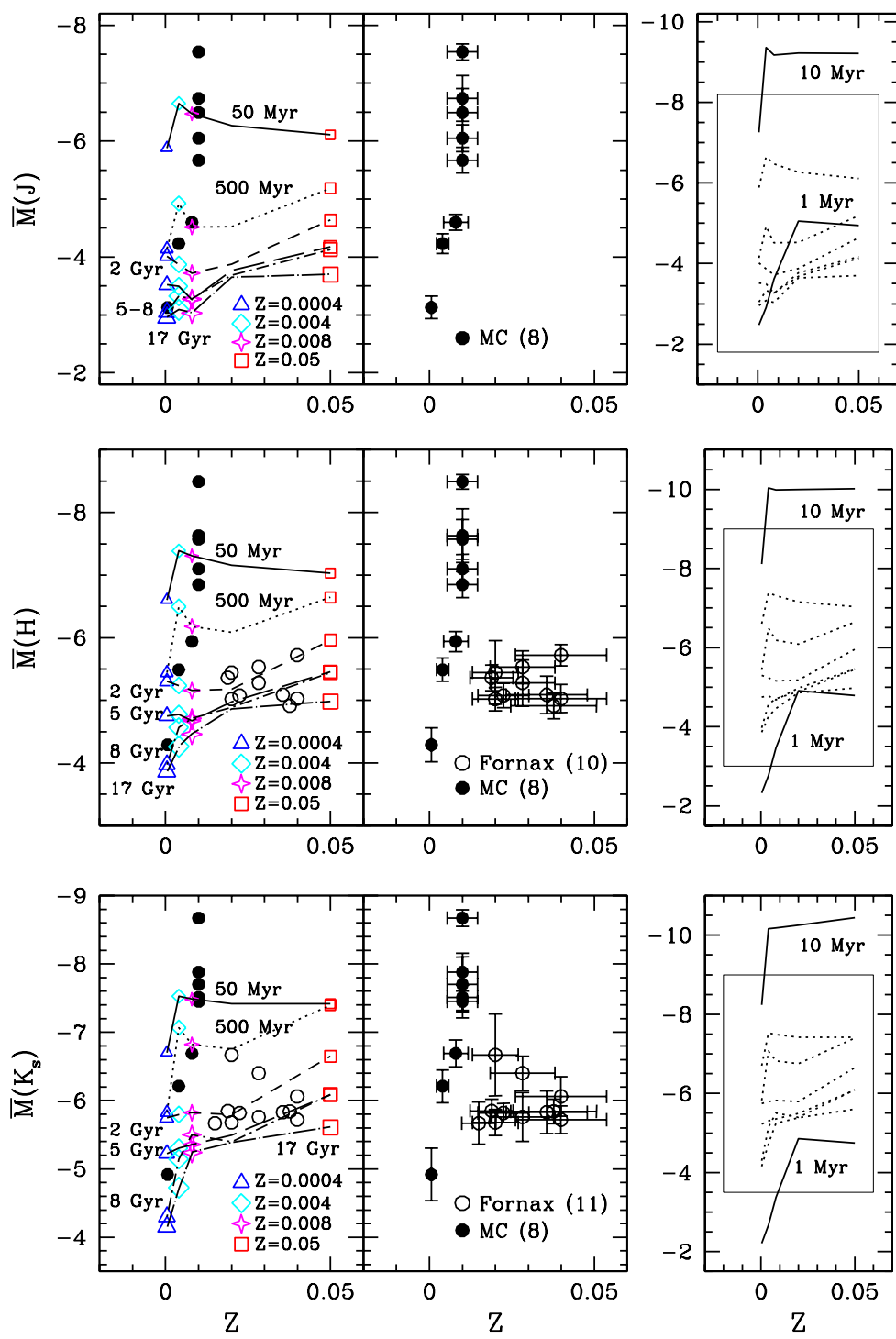


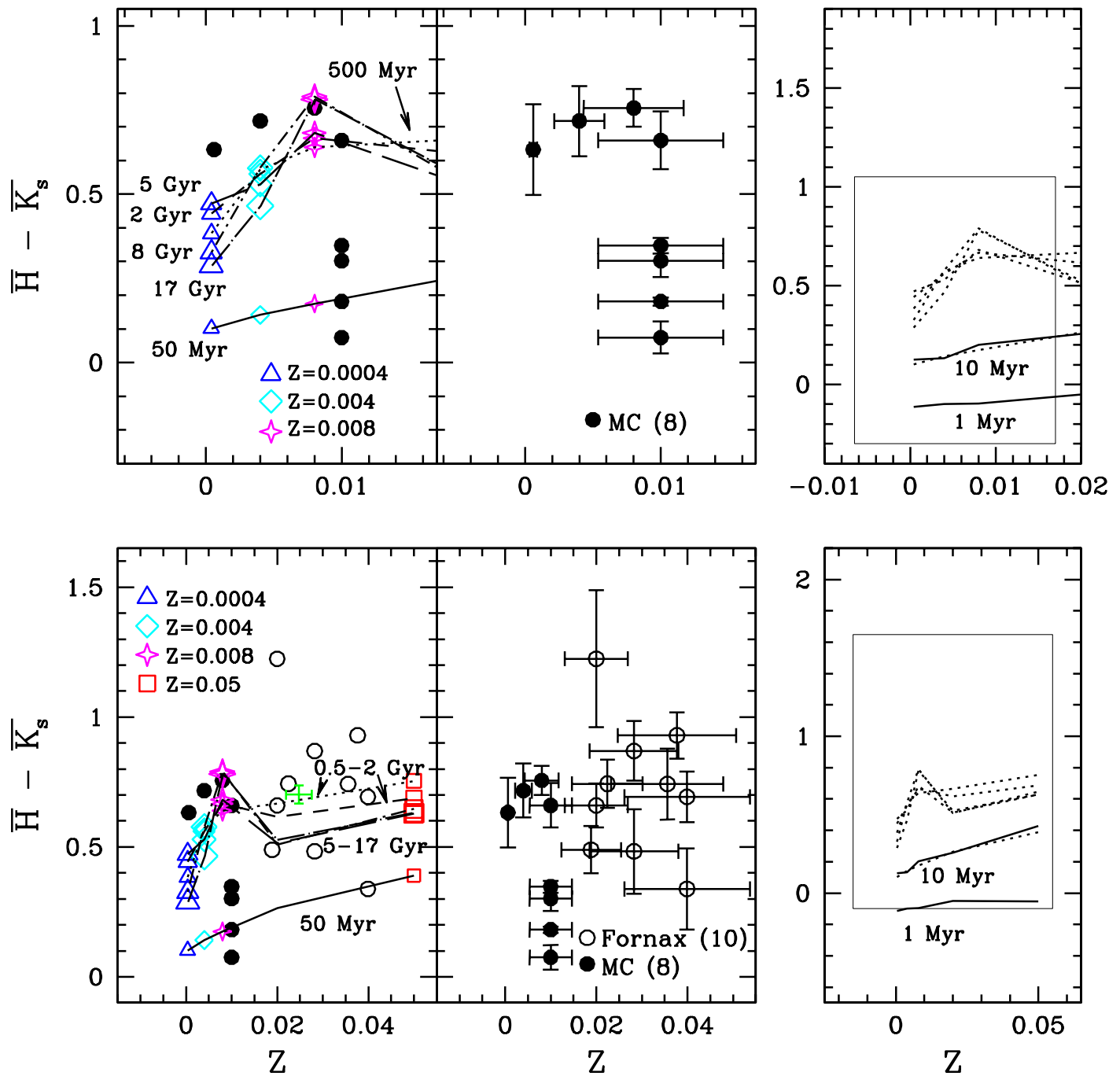












This figure "f2.jpg" is available in "jpg" format from:

<http://arXiv.org/ps/astro-ph/0404362v2>